AJP

ISSN : 0971 - 3093

Vol 25, No 3, March, 2016

ASIAN JOURNAL OF PHYSICS

An International Research Journal

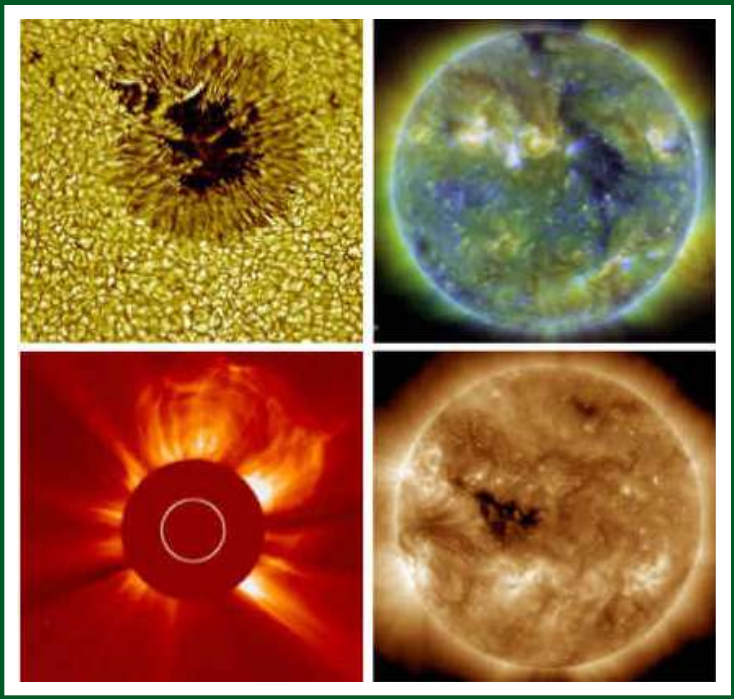

ANITA PUBLICATIONS

FF-43, 1st Floor, Mangal Bazar, Laxmi Nagar, Delhi-110 092, India

B O : 2, Pasha Court, Williamsville, New York-14221-1776, USA

ap

Asian Journal of Physics
Vol. 25, No 3 (2016) 233-265
Available on: www.asianjournalofphysics.in

Watching the Sun from space

W Dean Pesnell
NASA, Goddard Space Flight Center, Greenbelt, Maryland, USA

Space-based solar observatories have made fundamental discoveries about the lifecycle of the solar magnetic field and how that field affects the solar system. Observing the Sun from space provides access to all wavelengths of light and eliminates the smearing of atmospheric seeing. Being in space means the emissions from the highly-ionized material that are the natural emissions of the corona can be measured. Continuous observations of the Sun can be made from a single satellite in certain orbits. This leads to unexpected discoveries, such as orbiting coronagraphs showing that sungrazing comets are the most common class of observed comets. Or when the coronal holes discovered with the solar X-ray telescopes on Skylab explained long-noticed correlations in particle fluxes from the Sun with solar longitudes. Space-based coronagraphs and heliospheric imagers are able to track coronal mass ejections from when they leave the Sun until they hit the Earth or another planet. In a more practical point, as humans have become more entwined in the use of technology, the magnetic field of the Sun has become more intrusive. Energetic particles and high-energy photons from solar flares can compromise humans and electronics in space. As a coronal mass ejection passes by and interacts with the Earth's magnetosphere, it generates large currents at the Earth's surface that can disrupt power distribution systems. The measurements of Sun made possible by being in space will be described, along with some highlights of the observatories that make them.

Keywords: Solar satellites; Solar telescopes; Solar activity, solar spectral irradiance

1 Introduction

The Sun was used by our ancestors to track time and seasons; it was the source of radiation used to discover the spectral lines that led to quantum mechanics; and, because of its brightness, some of the first measurements made in space were of the Sun. Those observations showed that the ultraviolet and X-ray emissions of the Sun were related to solar activity, which comes from the solar magnetic field. Flares and coronal mass ejections (CMEs) are a direct result of the buildup of the magnetic field in the corona and chromsophere. Flares are a burst of energetic radiation and particles seen in X-rays and other wavelengths. CMEs are massive bursts of solar plasma and magnetic field that are sometimes ejected into space.

Many puzzles remain in our study of the Sun and solar activity. The causes of solar energetic events (SEEs, includes flares and coronal mass ejections), why is the corona hot, and the evolution of filaments are only three of them. For example, the ultraviolet and X-ray wavelengths available from space are the data needed to trace the energy flux and understand why the corona is hot.

Our exploration of the Sun from space began when a sounding rocket launched on 10-Oct-1946 recorded several solar spectra that measured the Mg II h & k lines from an altitude of 55 km, above the ozone layer but still below the O and O_2 absorption features that prevent extreme ultraviolet (EUV) light from reaching the ground [1]. The bright H I Lyman-α spectral line at 1215.7 Å was first observed in a spectrum on 12-Dec-1952 [2] and then in an image on 8-May-1956 [3]. These solar measurements provided the link between solar activity and changes in the terrestrial ionosphere [4], such as communication outages and radar

Corresponding author :
e-mail: William.D.Pesnell@NASA.gov (W Dean Pesnell)

interference. Sounding rockets were pointing the way to how the Sun affected the ionosphere but provided only a few minutes of observing time above the atmosphere. The first solar observatories in space began watching the Sun for longer periods of time.

Tousey [5] provides a summary of the first 20 years of solar ultraviolet research from space. He starts with the post-WW II sounding rockets and ends at the He II 304 Å spectroheliographic images from OSO II. In between was the birth of a new form of astronomy and solar physics.

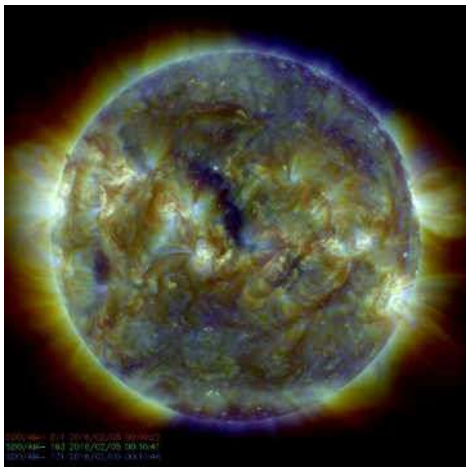

Fig 1. An image of the Sun on 6-Feb-2016 from AIA on SDO. Three EUV wavelengths, AIA 211 Å (red), 193 Å (green), and 171 Å (blue), were combined to give this image. Several solar features can be seen in this image, bright coronal loops, dark blue coronal holes, and darker filaments among them. Ground-based observatories can only see the filaments. Courtesy of NASA/SDO and the AIA science team.

Skylab was the beginning of the modern solar observatory in space. It carried several solar instruments that were pointed at interesting features by astronauts. Enormous progress has been made in space-based solar observatories in the four decades since the Skylab observations. This can be seen in Fig 1, where a recent AIA/SDO image displays the detail that is available from the current fleet of space-based solar observatories.

Most of the data from Skylab were recorded on film and analyzed after the film was brought back to the ground. Two developments have led to today's solar observatories in space. The first development was replacing photographic film by electronic detectors and high-speed radio telemetry as the way to send the data back to the ground. This freed imaging satellites from low-Earth orbit and allowed them to roam far into the solar system. This second came when the instruments stopped being research projects and the measurements became a data product. At that point solar scientists began to imagine what large imagers could do for the community rather than for only the scientists who built and ran the investigations.

The goal of this paper is to highlight the utility of solar measurements made from space rather than simply discuss the observatories that do those measurements. An article describing many of the missions is available from [6]. We shall first describe the instrumentation that is commonly used in space, followed by some of the successes of previous missions, and finally what the future may bring. All of the satellites that are mentioned are listed in Table 1, along with their launch and ending dates (as appropriate), and a website for further information or data.

Table 1. Selected satellite making solar measurements since 1973

Satellite	[1] Launch Date	[2]End Date	Website
Skylab	26 May 1973	8 Feb 1974	[3]http://nssdc/gsfc/nasa.gov/
AE C and AE E	16 Dec 1973	10 Jun 1981	http://nssdc/gsfc/nasa.gov/
P78 1	24 Feb 1979	13 Sep 1985	http://nssdc/gsfc/nasa.gov/
SMM	14 Feb 1980	2 Dec 1989	http://umbra.nascom.nasa.gov/smm/
Ulysses	6 Oct 1990	30 Jun 2009	http://www.cosmos.esa.int/web/ulysses
Yohkoh	30 Aug 1991	12 Sep 2005	http://solar.physics.montana.edu/ypop/
UARS	15 Sep 1991	14 Dec 2005	http://disc.sci.gsfc.nasa.gov/UARS
GOES 12-15	current fleet		http://www.ngdc.noaa.gov/stp/spaceweather.html
SoHO	2 Dec 1995	curr.	http://sohowww.nascom.nasa.gov
ACE	27 Aug 1997	curr.	http://www.srl.caltech.edu/ACE
TRACE	2 Apr 1998	21 Jun 2010	http://trace.lmsal.com
CORONAS-F	31 Jul 2001	6 Dec 2005	http://coronas.izmiran.ru/F/
TIMED	7 Dec 2001	curr.	http://lasp.colorado.edu/home/see/
RHESSI	5 Feb 2002	curr.	http://hesperia.gsfc.nasa.gov/rhessi3/
SORCE	25 Jan 2003	curr.	http://lasp.colorado.edu/home/sorce/
Hinode	22 Sep 2006	curr.	http://hinode.msfc.nasa.gov/
STEREO A & B	26 Oct 2006	curr.	http://stereo.gsfc.nasa.gov
CORONAS-Photon	30 Jan 2009	1 Dec 2009	http://coronas.izmiran.ru/F/
PROBA2	2 Nov 2009	curr.	http://proba2.sidc.be
SDO	11 Feb 2010	curr.	http://sdo.gsfc.nasa.gov
IRIS	27 Jun 2013	curr.	https://iris.lmsal.com
GOES-R	est. October 2016		http://www.goes-r.gov
Solar Probe Plus	est. July 2018		http://solarprobe.jhuapl.edu/
Solar Orbiter	est. October 2018		http://sci.esa.int/solarorbiter
Solar-C	est. October 2018		http://hinode.nao.ac.jp/SOLAR C/
Aditya-1	est. 2019 -2020		http://aditya.iiap.res.in
INTERHELIO-Zond	est. 2022		http://smdc.sinp.msu.ru/elana/experiments/interhelios/index.html

[1]Launch date is day of launch, not start of operations. Future missions show the estimated launch date.

[2]End date is loss of data collection.

[3]Website is a location for additional information on the solar measurements and links to science data. A link to http://nssdc.gsfc.nasa.gov/ takes you to the NSSDC main page. From there you search for the spacecraft of interest.

2 Why measure the Sun from space?

Measuring the Sun from above the Earth's atmosphere means removing atmospheric absorption (so all wavelengths of light can be measured) and the atmospheric distortion of the wavefronts (diffraction and telescope aberrations limit the spatial resolution.) The properties of particles at all energies, such as the composition and energy distribution, can be measured. Measurements of the vector magnetic field as it moves past a spacecraft provide a link back to the solar surface.

The electromagnetic spectrum is divided into bands that reflect the observability of each band. Figure 2 shows how the transmittance of the neutral atmosphere to the ground is zero for wavelengths less than 300 nm. There is also limited transmission to the ground for wavelengths longer than 15 μm. Also, radio waves with frequencies less than the plasma frequency of the F layer, where $N_e \sim 10^6$ cm^{-3} so that $\nu_p = 9\sqrt{N_e}$ kHz ~ 10 MHz, are reflected by the ionosphere and cannot be detected on the ground. This is a problem for observing the solar corona, which contains plasma with temperatures that can exceed 10^6 K and emits light at spectral lines in the extreme ultraviolet and shorter wavelengths. Gyromagnetic radiation from electrons moving along the coronal magnetic field in the outer corona can be at frequencies less than 10 MHz. Thus, except for a few forbidden lines such as Fe XIV 5303 Å and Thompson-scattered light in a coronagraph, much of the radiation from the corona is largely invisible from the ground. Many of the details in the corona, such as coronal loops and thermal emissions of flares, can only be seen in EUV emissions such as in Fig 1.

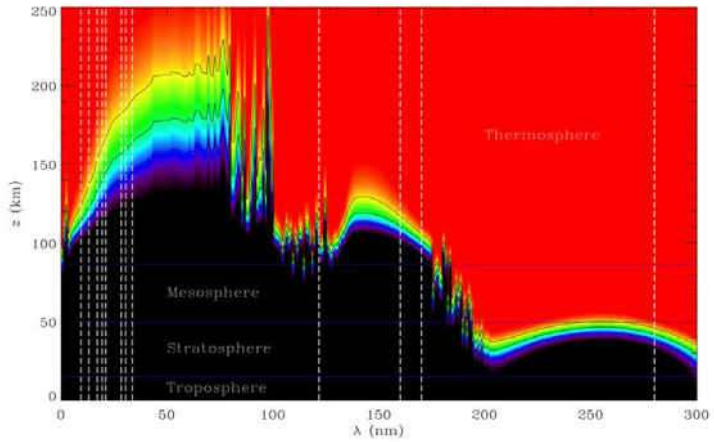

Fig 2. An illustration of the absorption of ultraviolet radiation in the terrestrial atmosphere. Red colors denote unattenuated solar radiation at that altitude and wavelength. Black regions are altitudes where light at that wavelength was completely absorbed above that point. Contours are drawn at 25%, 50%, and 75% absorption. Horizontal blue lines show the dividing lines for the named atmospheric layers. The absorption in the EUV occurs above 150 km altitude, making the solar emissions at those wavelengths critical to understanding the density and temperature of the thermosphere. The vertical dashed lines show the wavelengths of solar spectral lines often used in solar studies (AIA passbands plus Fe XV 284, Lα 1216, and Mg II 2800). The atmosphere becomes transparent just beyond the 300 nm limit of the ozone Huggins band in this figure.

Unlike the blackbody that dominate the visible wavelengths of the solar spectrum, the ultraviolet and X-ray wavelengths are dominated by spectral lines, with only a few weak continua. For example, the EUV spectrum measured by EVE/SDO from 27-Feb-2914 (solar maximum) shown in Fig 3 illustrates the complexity of the solar EUV spectral irradiance.

The solar X-ray and EUV emissions are absorbed through a complex photoabsorption spectrum to create the ionosphere and heat the thermosphere (Fig 2). The EUV energy is absorbed higher in the Earth's atmosphere than are X-rays, creating ions and electrons in the F-region ionosphere and heating the thermosphere. During a flare the X-ray irradiance increases dramatically. More radiative energy means a measurable change in the densities and temperatures within the ionosphere and thermosphere. Any increase in the density of the thermosphere increases the drag on satellites in low-Earth orbit. Some flares also show a long-lived increase in the EUV irradiance called a late-phase flare. Unfortunately, the duration is so long that any effects are masked by the normal diurnal variation. Research continues to see if late-phase flares are an

important component of space weather or simply an essential clue of how solar flares work.

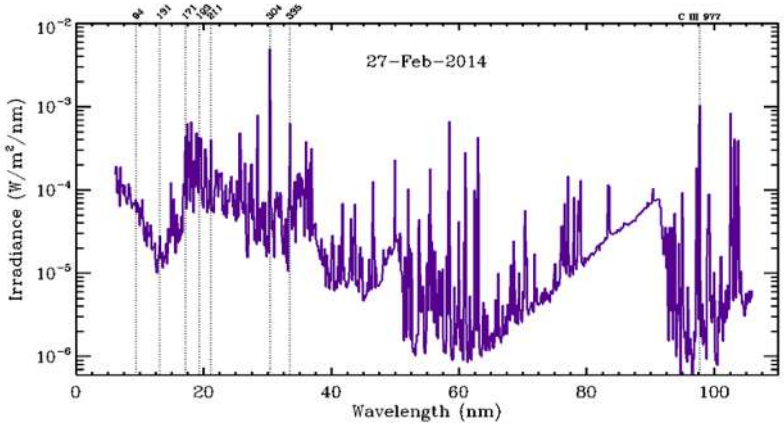

Fig 3. A day-averaged EUV spectral irradiance for 27-Feb-2014 as measured by EVE, plotted against the wavelength in nm. The seven AIA passbands are identified with vertical dashed lines. The He II 304 Å line is the brightest in this wavelength range, with the C III 977 Å line the next brightest. The total radiant energy in this spectrum, 5.3 mWm^{-2}, may only be about 10^{-5} times the total solar irradiance, but it is responsible for most of the ionization in the upper atmospheres of the Earth, Venus, Mars, and even Pluto. Courtesy: NASA/SDO and the EVE science team.

Once the importance of the solar EUV irradiance was recognized for producing both the terrestrial ionosphere and many of the effects now called Space Weather, attempts were made to measure the entire spectrum from X-ray wavelengths to 3000 Å. One series of instruments flew on AE-C, AE-D, and AE-E [7]. The reference spectrum from this data served the aeronomy community until the SEE instrument on TIMED was flown in 2001 and then EVE on SDO in 2010. That 20 years without EUV spectral irradiance data (the EUV hole) is illustrated in Fig 4.

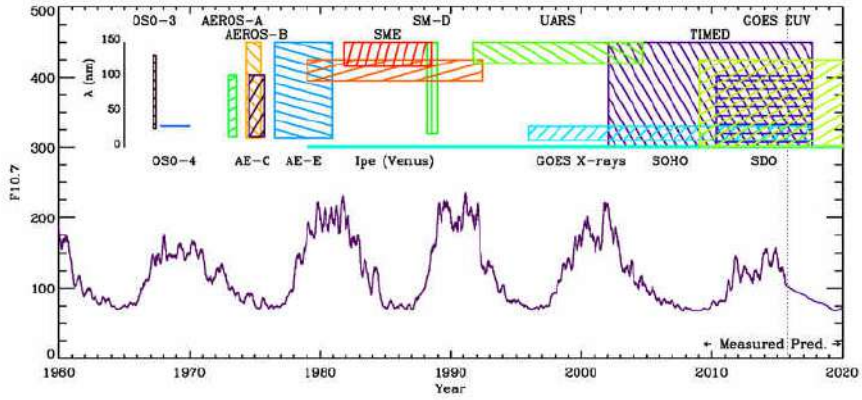

Fig 4. The history of measurements of the solar EUV spectral irradiance. The F10.7 solar spectral irradiance, a widely used measure of solar activity, is plotted as a solid line. Appended to that curve is a prediction of the remainder of Solar Cycle 24 from [8]. The spectral coverage of satellites that have measured the EUV spectral irradiance since the launch of OSO-3 in March 1967 is plotted above F10.7. The spectral coverage is shown by the height of the colored box (from 1 to 150 nm) although some missions provide measurements to longer wavelengths. The temporal coverage of each mission, taken from the NSSDC mission summary pages, is shown by the horizontal extent of the colored boxes. The end dates of the SoHO, TIMED, and SDO missions were set to end of the currently funded missions in 2017; the GOES X-ray and GOES EUV measurements are planned to continue until 2036.

Infrared observations of the Sun are less common from space. The opacity maximum of the negative Hydrogen ion (H^-) is near 1 μm in the solar atmosphere, which means emissions near this wavelength are highest in the solar atmosphere, while the opacity minimum of H^- near 2 μm is where the deepest layers of the atmosphere are visible. These wavelengths are visible from ground-based observatories. Even the Mg I 12 μm lines, the most magnetically sensitive line in the spectrum, can be observed from the ground. Far infrared observations of the Sun have been made from extremely dry locations, but no infrared observations of the Sun appear to have flown in space.

Radio observations of the Sun are recorded from Mercury to Pluto [9]. SWAVES (STEREO) has three receivers covering 10 kHz -16 MHz [10]. The low frequencies are near the plasma frequency at 1 AU ($N_e \sim 1$ cm^{-3}) while the higher frequencies measure the radio wave intensity, and the source direction and angular size from near the Sun ($N_e \sim 3 \times 10^6$ cm^{-3}) outward. SWAVES measures interplanetary Type II and Type III radio bursts. Type II radio bursts are associated with the propagation of CMEs in the corona and interplanetary medium. A CME-driven shock locally energizes electrons that generate radio emissions near the shock. As the shock moves outward into lower density, the emissions are generated at lower frequencies. Type II radio signatures provide a view of CMEs that complements the coronagraph images and in situ measurements. Type III bursts come from impulsively accelerated electrons streaming outward from the Sun along open field lines, and are often seen during the 4 days it takes for a CME to propagate to 1 AU.

Measuring the particle output of the Sun must also be done in space. Most energetic particles from the Sun are stopped by ionization cascades high above the surface of the Earth. Many satellites have measured these particles, as part of the thermal population of the solar wind, the energetic particles from flares, and the particles in a CME. The magnetic field must also be measured as the particles and field form a single entity. For a space weather forecaster it is the coupling of the solar magnetic field to the Earth's magnetosphere that energizes magnetic storms.

Only on rare occasions do the particles reach the surface. There have been only 72 of these so-called Ground-Level Events (GLEs) since February 1942. Using only GLEs to study the solar particle output is comparable to using only total solar eclipses to study the corona; a more complete picture is needed.

But every advantage comes with disadvantages. Satellites can be expensive to launch into orbit and operate. The amount of data that can be downlinked is often limited by availability of ground stations to receive the data. With two exceptions, the instrument hardware and electronics are frozen at the before-launch level and cannot be upgraded. The two exceptions were the Hubble Space Telescope (HST) and the Solar Maximum Mission (SMM). Astronauts replaced the attitude control mechanism and the main electronics system of the coronagraph on SMM, prolonging the mission by five years. HST had five servicing missions to install new instruments and repair broken electronics. However, the vast majority of space-based observatories are not reparable and future observatories will continue this tradition, especially those orbiting far from the Earth.

2.1 The Solar Corona

One part of the Sun benefits the most from space-based observations — the corona. Without space-based observatories the solar corona is difficult to see and understand. Total solar eclipses reveal the chromosphere and corona, but only about 2.4 happen each year. White-light coronagraphs image the electron density of the corona. Narrow-band coronagraphs can image some forbidden lines in visible wavelengths (such Fe XIV 5303 Å, same ion as AIA 211 Å, and Fe IX 4359 Å, the same ion as the various 171 Å imagers) that reveal details of the corona above the limb of the Sun. Neither technique can image the corona on the disk of the Sun. X-ray and EUV observations reveal the on-disk structures of coronal holes and coronal loops, the natural states of the corona. A comparison of the EUV and visible wavelengths during total solar eclipses is a comparison of excitation by electrons and resonant scattering very close to the limb of the Sun. Several

theories have been postulated to explain why the corona is so much hotter than the photosphere. Each uses a cascade of energy from the photosphere to the corona, whether nanoflares or resonant waves or through spicules [11]. All of the theories are tested with space-based data.

Effects of solar flares can be seen in ground-based Ca II H&K and Hα images. But it is observations from orbiting X-ray and EUV instruments that measure the high-temperature emissions of solar flares from the reconnection site. X-ray spectroscopy can resolve the motions of energetic particles after they are accelerated out of the reconnection site and strike material closer to the solar surface.

The size and evolution of the Sun's polar coronal hole is an example of the utility of space-based solar measurements. These coronal holes are dark patches surrounding the poles in EUV and X-ray images and are the longest-lived feature on the Sun. The Babcock-Leighton model of the solar dynamo stresses the importance of the polar regions during solar minimum as the seed of the activity in the upcoming Solar Cycle. Projection effects make this region difficult to observe and satellites that constantly observe the Sun can provide the measurements needed to understand this region.

3 Space-based observations of the Sun

Solar activity causes the radiative and particle output of the Sun to vary, from timescales of seconds to millennia and length scales from atomic to the entire solar system. Solar observatories measure how the radiative and particle output of the Sun varies. Much of this information can only be measured from space. We will now discuss some of the measurements that can be made from space. Some can be made from the ground but the majority can only be measured from outside the Earth's atmosphere.

3.1 Spectroscopy

Spectral lines from a wide variety of atoms, molecules, and ions are seen in the solar spectrum. They are created in an atmosphere where the temperature varies from a 6000 K thermal blackbody in the photosphere to the > 20 MK of flaring plasma in the corona and chromosphere. Those non-thermal regions come from the action of magnetic fields as they emerge from the photosphere. That means the study of the creation and destruction of the solar magnetic field dominates solar research and makes the study of the spectral lines emitted by the corona and chromosphere an intimate part of that study.

The Sun is an extended source of light and all the points along a spectrscopic slit will create a spectrum. Spectral lines in the photosphere can yield Doppler velocities of the bulk Sun and, by selecting a magnetically sensitive line, the magnetic field. Spectrometers with $\lambda < 300$ nm can measure the Doppler velocities in the chromosphere that go with the motions of spicules and the response of the chromosphere to flares (IRIS [12], EIS/Hinode, CDS, SUMER, and UVCS on SoHO, and UVSP/SMM). By using an imaging spectrograph these instruments are able to resolve the waves in the chromosphere, which have a shorter period than the p-modes in the photosphere.

Almost all of the instruments described below use a method of spectral filtering and could be described as spectrometers. Only coronagraphs and heliospheric imagers are typically designed to use unfiltered light.

3.2 Spectral Irradiance

The solar irradiance is the dominant source of energy to the Earth's atmosphere. Depending on the wavelength of the incident light, it heats the surface of the Earth, creates the ozone layer, creates the ionosphere, and heats the thermosphere. The total solar irradiance and short wavelength (X-ray, EUV, and UV) spectral irradiance are crucial measurements that are essential to our understanding of the Sun and Earth's atmosphere. X-ray and EUV photons are absorbed high above the Earth's surface and can only be measured from space. TSI must also be measured from space to capture the Wien tail of the photosphere and the shortwave emissions from solar activity. The total solar irradiance (TSI) tracks solar activity as well as the evolution of the Sun [e.g., the SORCE satellite, 13]. More detail will be given in Section 4.3 below.

The X-ray irradiance has been measured and used to classify the strength of solar flares by the GOES satellites since 1974. Figure 5 shows the X-ray irradiance during the latter half of the Halloween storms in October-November 2003. The indicated flare is the brightest ever recorded. Figure 2 shows that X-rays are absorbed by about an altitude of 100 km and must be measured from space.

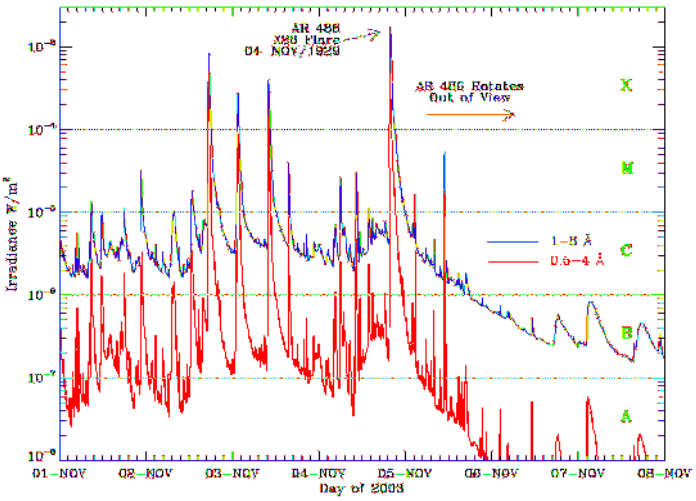

Fig 5. The GOES X-ray irradiances during the 2003 Halloween Storms, when Active Regions 486 and 488 produced numerous bright flares and CMEs that struck the Earth. These GOES measurements have been made since 1974 and are the primary classification of the strength of solar flares. The flare classes are the uppercase letters to the right (A, B, C, M, and X). Two features from AR 486 are highlighted, the X28 flare on 4-Nov-2003 and the loss of X-rays as the active rotates out of sight. Courtesy of the NGDC.

Solar EUV photons are produced by energetic electrons in a two-step process. First, the electrons must create highly ionized atomic ions in the corona; then they must excite the bound electrons of those ions.

Thus the presence of different ions acts as a thermometer of the coronal plasma. For example, Fe XII ions, which are seen in the AIA 193 Å passband, are created by higher temperatures than the Fe ix ions seen in the AIA 171 Å passband.

EUV radiation is a major source of ionization in planetary atmospheres as well as a probe of the solar corona. Solar EUV photons create ions and electrons when they are absorbed by neutral gas in a planetary thermosphere. Those ions can have lifetimes that exceed the length of a night. This results in a persistent yet time-dependent layer of ionization that can interfere with radio-based technologies. of the Sun increases during solar maximum, both due to flares and due to a slower varying background glow. The density of each planetary ionosphere and the temperature of the planetary thermosphere tend to track the solar cycle variation in the solar EUV output. Even with the utility of these measurements, the EUV spectral irradiance between 0.1 and 105 nm has been measured on only about 70% of the days since 1967 (Fig 4).

EUV instruments are extremely sensitive to contamination, notably from hydrocarbons. Any hydrocarbons that sublimates inside an on-orbit telescope will then condense onto the coldest part of the optical assembly — the detector. A layer of 70 nm of Teflon would attenuate the signal 50% at the 171 and 193 Å passbands (Fig 6). Other hydrocarbons have similar, and sometimes larger, absorption coefficients that vary with wavelength in unique ways. A strong contamination control program must be in place throughout the building EVE instruments to keep materials that could sublimate out of the optical path. Accounting

for the effect of condensed contaminants is done by cross-calibration with other on-orbit instruments and sounding rocket flights of similar instruments.

EUV instruments need extremely clean build environments

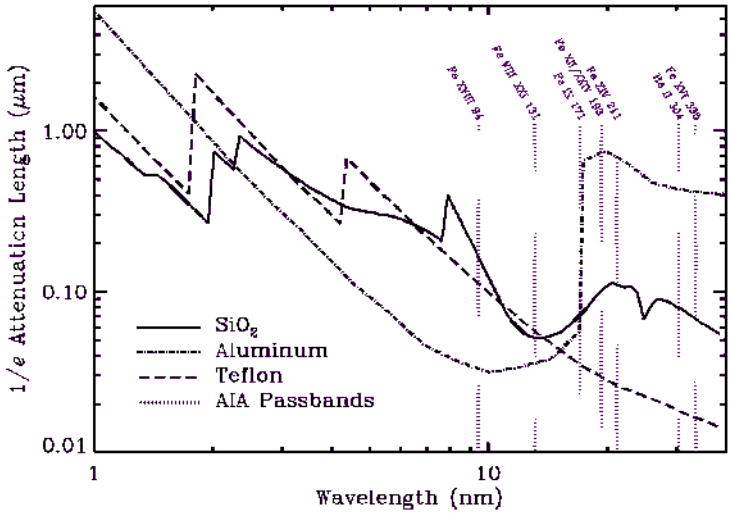

Fig 6. The 1/e attenuation lengths for SiO_2, Al, and Teflon. Values were obtained from the Henke coefficients at the webpage http://henke.lbl.gov/optical_constants/atten2.html. Vertical dotted lines are drawn at the wavelengths of the AIA/SDO EUV channels and labeled with the dominant ion species and wavelength. Note that Al cannot be used as a filter for the 94 and 131 Å passbands as even 25 nm of Al would attenuate the light by 50%.

The solar UV spectrum comprises the Wien tail from the photosphere and spectral lines that primarily come from the chromosphere, such as the Mg II 2800 lines. Ultraviolet wavelengths longer than 200 nm are absorbed lower in the Earth's atmosphere, principally by the ozone created by the absorption of even shorter wavelengths. The reflection of solar UV by ozone is used to measure the column density of the ozone layer. This also means that the solar UV irradiance has been measured for many years by satellites studying the ozone layer[1].

3.3 Imagers

While the solar irradiance is how the Sun directly affects the Earth, understanding the irradiance requires information about where it comes from. Solar imagers provide some of that information.

Solar imagers are often a type of spectroheliograph, an instrument that measures the brightness of a small wavelength band across the disk. Prior to 1940, these instruments used a prism or grating to disperse the spectrum perpendicular to a narrow slit that was then scanned across the Sun. The desired spectral line was then isolated and recorded either on photographic film or an electronic detector. The recorded strips were laid next to each other to build up the solar image. This is in contrast to a visible light imager that can use lenses and mirrors to bring an image to focus.

Imagers at EUV and X-ray wavelengths reveal coronal holes, prominences, and coronal loops; provide flare diagnostics; and can observe sun-grazing comets very close to perihelion.

[1] http://acd-ext.gsfc.nasa.gov/Data_services/merged/index.html

Plasma at temperatures of millions of Kelvin is the natural state of the solar corona. This material does not strongly emit in the wavelengths accessible to ground-based observatories. The few spectral lines that are available can be seen only on the limb by using an occulting disk or the Moon to block the blackbody radiation from the disk. Imagers in space can measure the resonance lines of the coronal ions in extreme ultraviolet and X-ray wavelengths. Full-disk images of coronal loops can be created.

Hard X-ray and γ-ray imagers cannot use conventional optics such as a lens or mirrors to form an image because the photons are absorbed rather than reflected by the normal optical surfaces. Instead, these telescopes consist of a series of aligned grids which form several collimated light paths. Each sub-collimator has a non-position-sensitive detector. The signal from each detector is then used to construct an image by computation. Yohkoh HXT [14] and RHESSI use these masks to image gamma rays. Grazing incidence mirrors were used for several solar instruments that flew on Skylab: S-020 [15]; S-054 [16]; S-055 [17]; S-056 [18]; S-082A [19]; S-082B [20] with an XUV monitor described in [21]. While some data on Skylab was examined and recorded electronically, most of the images were recorded on film and analyzed on the ground.

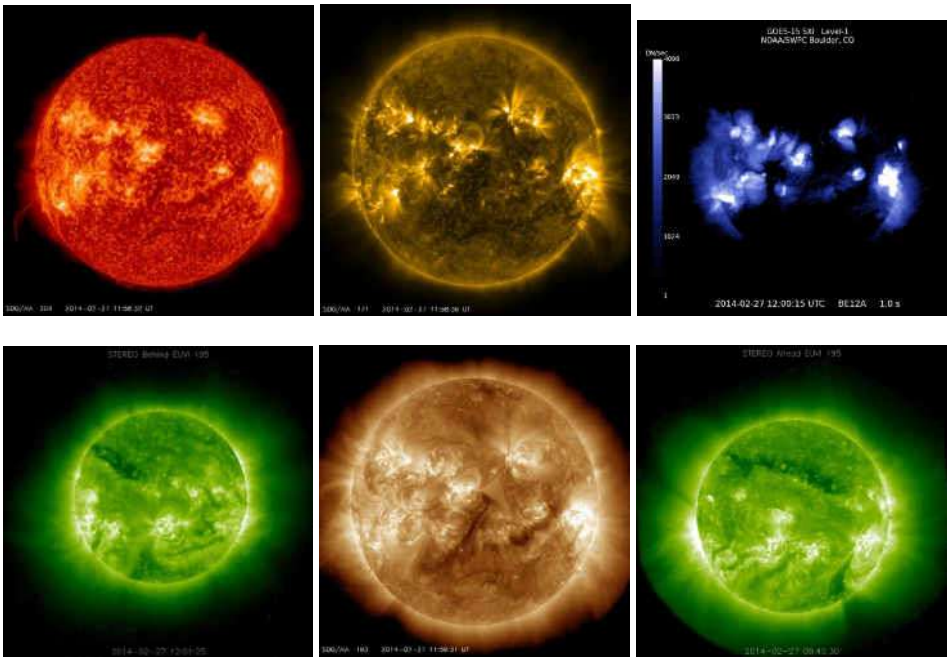

Fig 7. Views of the Sun at 1200 UTC on 27-Feb-2014, the day of maximum daily sunspot number in Solar Cycle 24. From left to right on the top row are AIA 304 Å, AIA 171 Å, and SXI BE12A 1.0 s images, in order of increasing temperature. You can see the active regions listed in Fig 8 as bright regions, with coronal loops extending above the limb from ARs 11959 and 11960. Coronal loops are seen above the other active regions as well. There is also a coronal hole in the center of the northern hemisphere and several filaments. The bottom row uses STEREO B 195 Å, AIA 193 Å, and STEREO A 195 Å images to show how the corona varies with longitude on the same day. Courtesy of NASA/SDO, the AIA and HMI science teams and SECCHI/STEREO.

Modern examples of grazing-incidence full-disk X-ray imagers include Yohkoh SXT, which sampled energies between 0.25 and 4 keV (a wavelength range of 0.3–5 nm) [22], and the SXI imagers flown on GOES 12–15 that image the Sun in wavelengths between 0.6 and 6 nm (an energy range of 0.2–2 eV) [23, 24]). SXI uses a image-intensified CCD as a detector. An example SXI image is in upper right corner

of Fig 7. Soft X-ray and EUV telescopes can be made using either glancing-incidence or multilayer, normal-incidence mirrors. Either type can be combined to form soft X-ray or EUV images of the Sun on a CCD sensor. The multilayer coatings can be tuned to produce the desired EUV wavelength bandpass. Examples of such telescopes include Mo/Si multilayer mirrors on EIT/SoHO [25], EUVI/STEREO [26, 27], and SWAP/Proba-2 [28, 29]; and the Mo/Si, SiC/Si, and Mo/Y multilayer mirrors on AIA/SDO [30]. Examples of AIA/SDO and EUVI/STEREO images are in the bottom row of Fig 7.

Photons at longer wavelengths must be blocked from any EUV detector as the visible irradiance of the Sun is about 10^6 times the EUV irradiance. Aluminum foils can be used to reflect the visible and IR wavelengths while passing the EUV wavelengths longer than the 17 nm absorption edge of the Al *L* shell (see Al curve in Fig 6). Other metals are available to provide short-wavelength blockers at other edges. Multilayer mirrors reflect light at higher orders and placing foils in front of the telescope removes bright spectral lines that would contaminate the images in higher order reflections.

3.4 Magnetograms

Magnetograms provide direct evidence of the solar magnetic field and how it is converted into solar activity. They are created by measuring either the Zeeman or Hanle effect in a spectral line. Both effects come from the interaction of the electron energy levels in atomic ions with the magnetic field. In the Zeeman effect, the energy levels are split about the zero-field value and polarized. A spectral line in absorption would have circularly polarized components whose separation is sensitive to the magnetic field component along the line of sight to the observer and linearly polarized components that can be interpreted to give the full vector magnetic field. The Zeeman effect increases with wavelength and can be used to measure large fields in visible and infrared spectral lines. MDI/SoHO and HMI/SDO have used the Zeeman effect to measure the photospheric magnetic field for over twenty years.

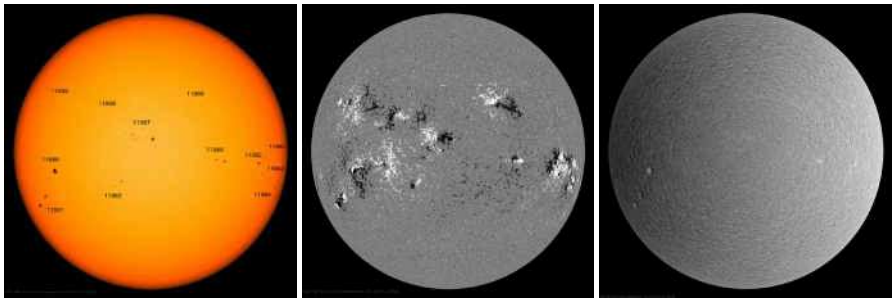

Fig 8. Three views of the Sun at 1200 UTC on 27-Feb-2014, the day of the maximum daily sunspot number in Solar Cycle 24. From left to right are an intensity image, a LOS magnetogram, and a Dopplergram from HMI. Each image is oriented with the solar north rotation axis at the top of the image. The color scale for the magnetogram uses white for field pointing toward the observer and black for field pointing away. Several active regions are identified in the intensity image. The Dopplergrams are displayed with red shifts in black and blue shifts in white. You can see several active regions in the Dopplergrams. You can also see several regions of strong magnetic field that cannot be seen in the other two images, especially in the Northern hemisphere. Courtesy of NASA/SDO and the HMI science team.

The Hanle effect involves phase-coherent interference patterns between energy levels that are weakly perturbed by the magnetic field. It produces linearly polarized light and gives either the strength of the magnetic field (in weaker fields) or its direction (in stronger fields). The Hanle effect could be used in ultraviolet resonance lines to measure the much weaker field strengths fund in the chromosphere and corona. Several missions have proposed using the Hanle effect in Mg II 2800 to study the weak magnetic fields of the quiet Sun that the Zeeman effect cannot resolve imaging magnetographs can be constructed from Fabry-Perot elatons or Michelson interference filters. By changing the polarization properties of the light passing

through the interferometers a narrowband filter can be produced that scans across a spectral line at each point on the solar disk. Measuring the Stokes parameters of the spectral line allows the magnetic field to be derived at each point as well. Full-disk magnetograms have been produced by ground-based observatories such as GONG and the satellite instruments MDI/SoHO and HMI/SDO (see the center panel in Fig 8.) Hinode also produced small-scale maps of the solar magnetic field.

Magnetograms also provide the boundary conditions for magnetic field models that extrapolate the surface magnetic field into the corona and heliosphere. The complexity of the magnetic field is contained within magnetograms. There is evidence that changes in the vector magnetic field can provide predictions of solar flares and the filament eruptions that are the initial stages of CMEs.

Full-disk magnetograms represent a tradeoff between the spectral resolution of the filtergrams and the desired temporal resolution

3.5 Dopplergrams

Dopplergrams are a display of the line of sight velocity as measured by the Doppler shift of a photospheric spectral line. The measured velocities are analyzed, often through spatial and temporal transforms, to give a wave spectrum. That wave spectrum is a probe of the solar interior, imaging the interior flow fields and nascent active regions. Newer techniques, such as time-distance helioseismology, use the scattering properties of the waves to measure the effects of magnetic fields near the surface.

A Dopplergram is produced by measuring the Doppler shift in pixels spanning the disk and plotting them as an image. The same interference filters that produce magnetograms can also be used to measure the Doppler shift. Full-disk Dopplergrams have been produced by ground-based observatories such as GONG and the satellite instruments MDI/SoHO and HMI/SDO (see the right panel in Fig 8).

Dopplergrams are an integral part of our understanding of the solar convection zone, the seat of the solar dynamo. Just like seismic waves on the Earth can be inverted to tell us about the interior of the Earth, the solar p-modes can be inverted to measure conditions inside the Sun. Additional analyses can show local changes that may indicate where an active regions is about to erupt. Other patterns seen in the Dopplergrams include differential rotation, supergranulation (which tracks conditions in the outer part of the solar convection zone), and giant cells.

Dopplergrams require an extremely accurate ephemeris so the orbital velocity can be accounted for in the data

3.6 Coronagraphs

A coronagraph is usually a white-light telescope with an occulter disk designed to block the direct light coming from the solar disk. This allows the extremely faint emission from the solar corona to be imaged. A coronagraph image from 27-Feb-2014 is shown in Fig 9. Coronagraphs see light scattered from the free electrons in the corona. The density of electrons in the corona is quite small and the scattered light is about $10^{-6}\times$ the photospheric irradiance. This means the scattered light within the telescope must be well-controlled, especially any light scattered from the occulting disk. Heliospheric imagers (HIs) are modern adaptations that also use occultation and a baffle system to create wide-angle views of the heliosphere. The HIs on STEREO achieve light rejection levels sufficient to view the diffuse density enhancements in the solar wind plasma from near the Sun to past 1 AU. The first HI was flown as the SMEI on Coriolis[2].

Coronagraphs and HIs provide images of the solar wind as it flows through the solar system [31]. A CME trajectory can be derived to predict whether it will strike the Earth or other planets. Space weather prediction centers use this information to anticipate the satellite outages and power distribution problems

[2]http://smei.ucsd.edu/new_smei/indes.html

created when a CME hits the terrestrial magnetosphere[3]. Data from coronagraphs drives models of the solar wind with ever-increasing fidelity. A community effort was used to predict space weather effects that would be present during the encounter of New Horizons with Pluto[4].

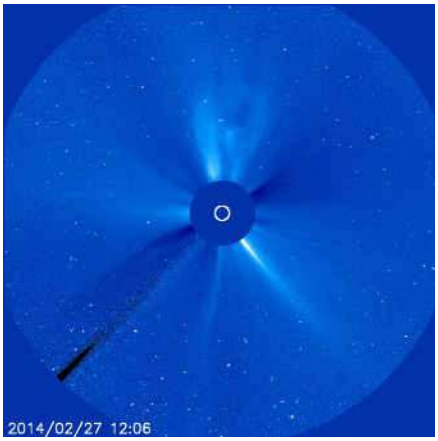

Fig 9. A LASCO C3 image of the outer corona of the Sun at 1206 UTC on 27-Feb-2014, the day of the maximum daily sunspot number in Solar Cycle 24. A CME is erupting at the top of the Sun. A bright streamer is moving out upward at about 4 o'clock. The dark area in the lower right is the spar that holds the occulting disk to block the direct sunlight. A white circle is drawn on the occulting disk to show the location and size of the Sun. Courtesy SoHO (ESA&NASA).

Most coronagraphs can also see the flotsam and jetsam of the solar system — comets and dust. They have been prolific discoverer of comets. Most of these comets are sungrazers, whose orbits take them very close to the solar surface, where they evaporate, breakup, and disappear. When SOLWIND began operating in 1979 there were 800 known comets[5], including 14 sungrazers. At the end of 2015 there are about 5400 known comets, making coronagraphs the discoverer of 56% of known comets and promoting sungrazers to over 60% of known comets.

Coronagraphs also serve the planetary community by measuring how dust moves through the solar system. Dust is constantly created by collisions of asteroids and moves toward the Sun. Sungrazing comets are another source of dust as they breakup near the Sun. Coronagraphs see light scattered from the dust as a function of the angular distance from the Sun. The scattered light provides information about the sources and dynamics of the dust. Astronomers also use coronagraph data to study variable stars.

Coronagraphs and heliospheric imagers in space have less scattered light far from the occulting disk

3.7 Particles and Fields

Particle and field instruments provide in situ sampling of the solar wind particles and magnetic field that have escaped the Sun. Scientific topics addressed by these instruments include the sources, acceleration mechanisms, and transport processes of these particles. They allow detailed studies into how the solar magnetic field links from the Sun into space; how the particles are accelerated and propagate around the Solar System, including to the Earth; and how the corona and solar wind are heated and accelerated.

---

[3]http://www.swpc.noaa.gov, http://iswa.ccmc.gsfc.noaa.gov/iswa/iSWA.html
[4]http://ccmc.gsfc.nasa.gov/missionsupport/NewHorizons_support.php
[5]http://www.johnstonsarchive.net/astro/sspopsgraph.html

These measurements are complicated by the need to coverage a enormous range of particle energies, including beaming motions, in the coordinate system of the local magnetic field. Hence, a magnetometer is needed to make high-precision *in situ* measurements of the heliospheric vector magnetic field.

To cover the energy range of the particles often requires several detectors where each is sensitive to a different population of particles. Some plasma instruments measure the ion and electron bulk properties (including the density, velocity, and temperature) of the solar wind. In addition to determining the bulk properties of the wind, these instruments can measure the solar wind ion composition for elements such as C, N, O, Fe, Si or Mg. Energetic particle detectors must measure the composition, timing and distribution functions of suprathermal and energetic particles.

A radio receiver can work as both an *in situ* and remote-sensing instrument. The remote sensing works as described above while the *in situ* mode uses multiple antennas to make simultaneous measurements of the vector magnetic and electric fields at a high time resolution. Combining these measurements can determine the characteristics of the electromagnetic and electrostatic waves in the solar wind.

The interplanetary magnetic field is very weak (~ 1 nT) so particle and field measurements require an environment with few stray magnetic fields to allow the IMF to be accurately measured.

It is good to have several types of measurements being made of the same event at the same time. Images of the full disk provide valuable data by themselves but also context for highly magnified views. The Trace spacecraft conclusively demonstrated that small scale structures are responding to influences outside the field of view of the instrument, which requires another imaging telescope to detect. Space-based Dopplergrams and magnetograms also benefit from having full-disk observations. This simplifies the operation of the instruments while presenting the scientists with evenly spaced data for optimum science.

4 Highlights from Past and Current Solar Satellites

Many solar missions have flown in space, there are 86 listed in [6]! Initially they were small, short-lived missions designed to understand what solar measurements could be made. As our appreciation for the effects of solar activity on planets and humans grew, so did the complexity and longevity of the missions. A list of the scientific papers and research supported by these missions would be extremely long. Here we list several past and current satellites, along with a few highlights from each, mostly related to the measurements described above. A mapping of the solar instrumentation classes on each satellite in Table 1 is shown in Table 2.

4.1 Skylab

Skylab, the first US space station, was launched into low-Earth orbit on May 14, 1973. Three crews manned Skylab between May 25, 1973 and February 8, 1974. Skylab included eight separate solar experiments on its Apollo Telescope Mount, five shortwave imagers, a white light coronagraph, and two Hα telescopes. S-056 was a grazing incidence X-ray telescope that produced images of the Sun in wavelengths from 6 to 49 Å. Images were taken through 6 different filters and recorded on film that was returned with the astronauts to Earth for processing. A movie[6] of these images shows some of the discoveries made from Skylab including coronal holes and X-ray bright points. Coronal holes are seen as dark regions in which the hot coronal material has a very low density and whose magnetic field are open to the heliosphere (Fig 10). Coronal holes were observed to rotate fairly rigidly and maintain their shape through several 27-day solar rotations in spite of the variations in rotation rate of the solar surface. X-ray bright points are small, compact,

[6]http://solarscience.msfc.nasa.gov/images/skylab.mpg

short-lived brightenings that are most easily seen in the coronal holes themselves. Coronal holes and bright points in several shortwave bands are still researched today.

Table 2. Selected satellites making solar measurements since 1973

Satellite	Irrad.[1]	Imaging[2]	Magnet.[3]	Doppler.[4]	Corona[5]	P.F. & W.[6]
Skylab		Yes				
AE C and AE E	Yes					
P78 1					Yes	
SMM	Yes	Yes			Yes	
Ulysses						Yes
Yohkoh		Yes				
UARS	Yes					
GOES 12-15	Yes	Yes				
SoHO	Yes	Yes	Yes	Yes	Yes	Yes
ACE						Yes
TRACE		Yes				
CORONAS-F	Yes	Yes				Yes
TIMED	Yes					
RHESSI		Yes				
SORCE	Yes					
Hinode		Yes	Yes			
STEREO A & B		Yes			Yes	Yes
CORONAS-Photon		Yes				
PROBA2	Yes	Yes				
SDO	Yes	Yes	Yes	Yes		
IRIS						
GOES-R	Yes	Yes				
Solar Probe Plus					Yes	Yes
Solar Orbiter		Yes			Yes	Yes
Solar-C		Yes				

Notes:

[1]Irradiance includes the total solar irradiance and spectral irradiance.

[2]Imaging in any passband (primarily EUV and X-ray).

[3]Magnetograms

[4]Dopplergrams

[5]Coronagraphs and heliospheric imagers can measure any wavelength.

[6]Particles, Fields, and Waves for solar output. Satellites in low-Earth orbit measure mostly the magnetosphere and those instruments are not included

Skylab re-entered the Earth's atmosphere over Australia in 1979. It had been anticipated that Skylab would remain in orbit for at least 10 years. The shorter life was caused by Solar Cycle 21 rising to maximum faster than anticipated by the solar activity predictions used at launch. As a result this re-entry has become a case study in solar activity predictions. Even now, anticipating the level of activity in the next sunspot cycle

remains an unsolved problem. Predictions of Solar Cycle 24 had a wide spread in values, in part related to the same discussion for Solar Cycle 21 – what information to keep and what to leave out of the correlations used for the predictions [32].

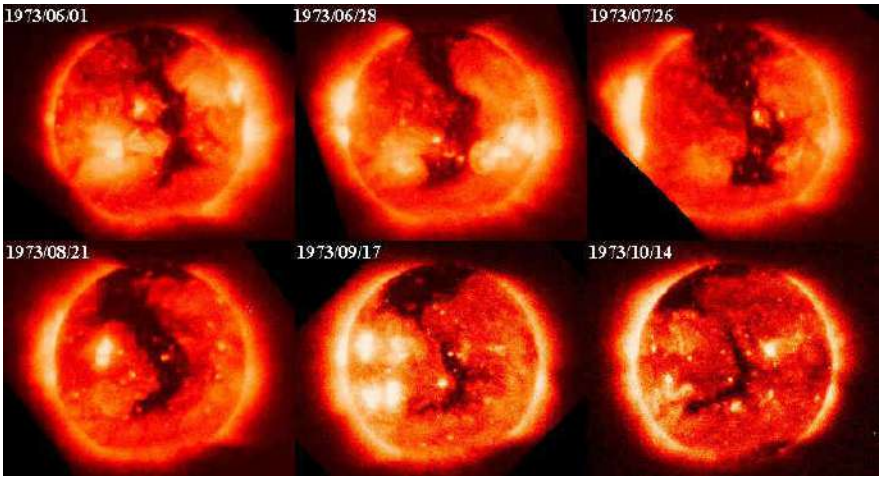

Fig 10. A long-lived coronal hole seen by S-056/Skylab over six successive rotations. The elongated dark path starting near the top of the image (the solar North pole) and spreading toward the middle (the solar equator) is the coronal hole. The hole could be identified for about four months. Image is from http://solarscience. msfc.nasa.gov/images/skylab_coronal_hole.jpg.

4.2 P78-1

P78-1 was launched into a Sun-synchronous orbit at 0824 UTC on 24-Feb-1979. P78-1 used an OSO bus with a rotating wheel section to provide stability and a solar-oriented sail that held some of the instruments. It carried a white-light coronagraph, an extreme-ultraviolet imager, an EUV spectrometer, an X-ray spectrometer, an X-ray monitor, and a gamma-ray spectrometer. The white-light coronagraph and the ultraviolet imager were combined into a package called SOLWIND. The ultraviolet imager used a CCD, one of the first uses of a CCD in space.

Major science highlights of P78-1 were the first observations of halo CMEs, a CME that is heading straight for the Earth that is seen as a bright ring around the occulting disk, and the discovery of the association of CMEs with interplanetary shocks. Deducing that a halo CME was coming towards (or directly away from) the Earth is a milestone in associating space weather effects with CMEs and predicting when those effects will arrive.

P78-1 also recorded high-quality and high-spectral-resolution X-ray spectra of flares and active regions at wavelengths less than 25 Å. Measurements of the spectral irradiance in four X-ray bands allowed the Doppler signature of chromospheric evaporation on X-ray line profiles to be first reported. P78-1 also contributed some of the first observations of γ-ray bursts.

The SOLWIND coronagraph was the first space-based instrument to discover a comet, which was a Kreutz sungrazer. The nine comets discovered by SOLWIND started a long tradition of space-based coronagraphs discovering sun-grazing comets.

The satellite operated until it was destroyed in orbit on September 13, 1985 by a test of the ASM-135 anti-satellite missile.

4.3 Solar Maximum Mission

The Solar Maximum Mission (SMM) was launched at 1557 UTC on February 14, 1980. SMM

carried a suite of instruments designed to study solar activity with a concentration on flares. These instruments were the Active Cavity Radiometer Irradiance Monitor (ACRIM 1), the Coronagraph/Polarimeter (C/P), the Ultraviolet Spectrometer and Polarimeter (UVSP, a UV imaging spectroheliograph), the Gamma-Ray Spectrometer (GRS), the soft X-Ray Polychromator (XRP), the Hard X-ray Imaging Spectrometer (HXIS), and the Hard X-Ray Burst Spectrometer (HXRBS).

One science highlight from SMM was the discovery that the Total Solar Irradiance (TSI) varied in phase with the sunspot number. ACRIM 1 measured TSI from 1980–1989. The accuracy and precision of the data was sufficient to show that the Sun is brighter during solar maximum than solar minimum [33]. The faculae and network contributions that brighten during solar maximum overcome the radiative loss caused by the dark sunspots moving across the disk. Given the long and contentious history of ground-based measurements of the solar "constant," the result of a brighter Sun at solar maximum had to withstand quite a lot of criticism. It was essential that data from another instrument (at first ERB on Nimbus 7) was available to verify and validate the ACRIM measurements [34]. TSI has since been measured by ERB/ERBS, ACRIM/UARS, Virgo/SoHO, ACRIM/ACRIMSAT, and TIM/SORCE. A composite time-series using data from several satellites is shown in Fig 11, along with the sunspot number.

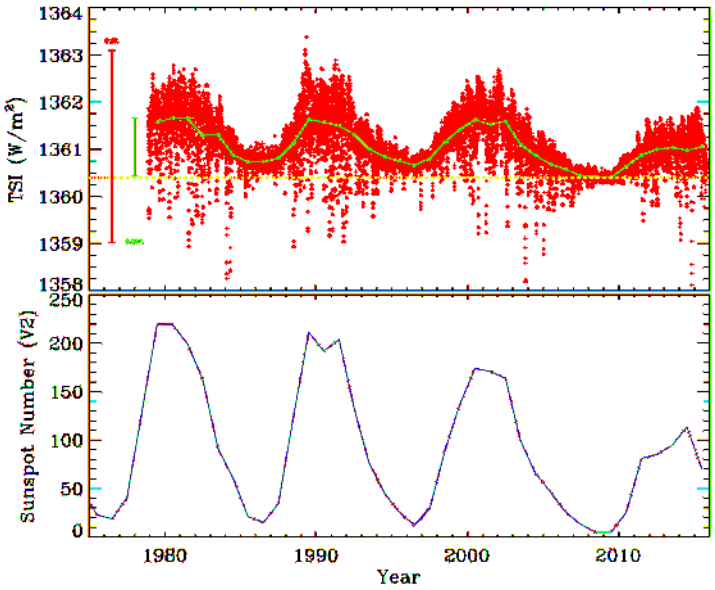

Fig 11. A composite of TSI measurements as derived by the PMOD group at the World Radiation Center in Davos, Switzerland [35]. The top plot shows the daily TSI values in red and the annual-average TSI in yellow. The dashed yellow line is the minimum in the solar minimum of 2008. The error bar in red shows a peak-to-peak variation of 0.3%, which captures most of the variation in the daily data. The error bar in yellow shows a peak-to-peak variation of 0.09%, which captures all of the variation in the annual data. The lower plot shows the annual average of the new calibration of the sunspot number.

Not all of the variations of TSI are understood. One example is the lower averaged TSI value in the 2008 solar minimum compared to the previous two solar minima. Another is how the small variations in TSI could cause significant changes in the terrestrial climate, if variations in the thermal input from the Sun have caused climate changes in the past.

Other results from SMM included the discovery by UVSP of acoustic waves propagating through the transition region above sunspot umbras. These waves could be a coupling between the p-modes in the

photosphere and the chromosphere. These waves have since been observed in Trace, Hinode and SDO data. Many models have been developed to explore the link between acoustic waves and magnetic fields. A review of progress in our understanding of these waves is in [36].

The coronagraph on SMM discovered 10 more comets (all sungrazing) between October 1987 and October 1989.

4.4 Ulysses

Ulysses was launched from the Space Shuttle Discovery at 1147 UTC on 6-Oct-1990 into a deep-space orbit. A Jupiter fly-by was used to change the inclination to 79°, allowing it to fly over the solar poles. It carried 13 instruments to measure the plasma properties, magnetic fields, interplanetary dust, and radio waves at the spacecraft.

Ulysses made nearly three complete orbits of the sun. The high inclination orbit gave Ulysses a unique view of the polar regions of the Sun. The probe measured the three-dimensional character of galactic cosmic radiation, energetic particles produced in solar storms and the solar wind. Ulysses allowed scientists to map the constituents of the heliosphere in space, while its longevity enabled them to observe the Sun over almost an entire 22-year solar cycle.

Although Ulysses did not carry any imagers, it made *in situ* measurements that showed coronal holes, in particular the polar coronal holes, are sources of the fast solar wind, while the slower solar wind comes from active latitudes. A steady decrease in the strength of the magnetic field coming from the Sun's polar regions was observed. This was similar to the decreases measured by ground-based observatories and, towards the end of the mission, marked the smallest magnetic fields in the last 200 years. Among other discoveries, Ulysses data was able to show a disagreement between the solar wind and photosphere in the relative abundance of oxygen and hydrogen [37], with the solar wind being 25% larger. Oxygen is a critical element in the Sun and Earth, so an accurate knowledge of its relative abundance is essential to our understanding of the solar system and universe.

With an aphelion distance of 5 AU, Ulysses flew too far from the Sun to rely on solar panels for electric power. Radioisotope Thermal Generators (RTGs) were used to provide power to the spacecraft. The RTG output power steadily decreased with time and, after the third polar pass, was insufficient to keep the propellant used for maneuvers from freezing. Ulysses was commanded to power off the spacecraft on 30-Jun-2009 and became another small object orbiting the Sun.

4.5 Yohkoh

Yohkoh was launched as Solar-A at 0230 UTC on 30-Aug-1991 into a low-inclination low-Earth orbit. It was renamed Yohkoh (Japanese for Sunbeam) upon commissioning. It carried two X-ray telescopes, and two high-energy spectrometers. The Soft X-ray instrument (SRT) combined a grazing-incidence telescope with a CCD to measure photons with energies from 0.25–4 keV.

Yohkoh data was used to identify several different classes of flares. It was able to show that the solar corona was much more dynamic and active than had previously been supposed, even far from regions of peak activity. Yohkoh observed almost an entire solar cycle before it went into standby mode during annular eclipse in 2001. It was destroyed during re-entry in 2005.

4.6 SoHO

The Solar and Heliospheric Observatory (SoHO) was launched at 0808 UTC on 2-Dec-1995 into an orbit at the Sun-Earth L1 Lagrange point. SoHO has been one of the most important solar missions to date. From the Sun-Earth L1 point, SoHO has an uninterrupted view of the Sun at many wavelengths and samples the particles and interplanetary magnetic field upstream of the Earth. An example of how the solar corona

varied over the SoHO mission is shown in Fig 12. The dim corona with distinct polar caps in 1996 gives way to brighter and more structured corona of the 2001 maximum of Solar Cycle 23. The next cycle gets started in 2010 and reached a maximum in 2014. The changes in the polar regions can be compared to those in the mid-latitude active regions to see the out-of-phase behavior of the two regions.

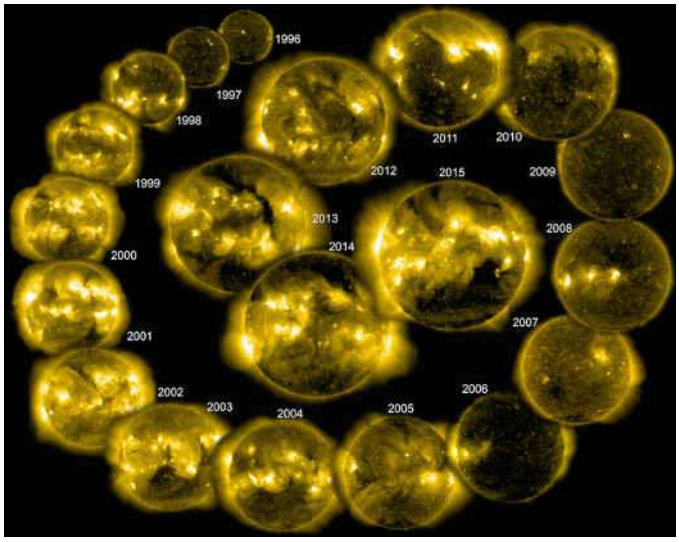

Fig 12. The changing face of the EUV Sun from twenty years of observations in SoHO's EIT 284 Å passband. Since launch, SoHO has watched the waxing and waning of the Sun's corona in four EUV passbands and three coronagraphs. These images, taken at the beginning of April each year, show the changes of the lower corona over almost two sunspot cycles. Courtesy SoHO (ESA & NASA).

There have been many science highlights from SoHO. Time-distance helioseismology was developed by researchers as another way to look inside the Sun using the acoustic waves from MDI Dopplergrams. Other methods, such as holography and ring diagrams, were then developed to look at different details of the solar interior [38]. By extending the methods to the GONG data, the MDI results could be verified and systematic errors isolated. MDI data was used to study the large-scale internal flows that continue to the present with HMI/SDO. Flux transport models of the solar dynamo rely on these measurements to constrain the internal velocity fields that generate and advect the solar magnetic field. These models were developed into a predictive capability for Solar Cycle 24, the first new prediction method in several cycles. The descendants of these models have made considerable progress in our understanding of how the solar dynamo works.

SoHO also made significant studies in the interaction of solar eruptive events, such as flares and CMEs, with the heliosphere. Three nested white-light coronagraphs (LASCO) and another that observed in Lα and O VI 1032 (UVCS), ensured that what left the Sun was being observed.

SoHO was watching when a series of large flares and CMEs were produced by active regions 486 and 488 between 19-Oct-2003 and 07-Nov-2003. Several large flares were produced by these active regions, including the largest ever recorded, an X-45 flare on 4-Nov-2003 (see Fig 5). Some images of what the Sun looked like during the Halloween storms are shown in Fig 13. The particle and fields instruments then measured what arrived at SoHO, sometimes several days after the event.

LASCO has discovered more comets than any other instrument — over 3000 at the end of 2015. These comets are mostly tiny sungrazing comets that evaporate and disintegrate as they near the Sun.

SoHO is still going strong after 20 years of on-orbit operations. It did survive a three month outage when the spacecraft turned away from the Sun and lost power. It was successfully restored to full capability once it had moved around the Sun and the solar panels began to generate power.

4.7 TRACE

The Transition Region and Coronal Explorer (TRACE) was launched at 0243 UTC on 2-Apr-1998 into a sun-synchronous orbit. TRACE carried a single normal-incidence telescope with different multilayer filters in each quadrant of the primary mirror and a CCD. EUV filters (Fe IX 173 Å, Fe XII 195 Å, and Fe XV 284 Å) occupied three quadrants while four UV wavelengths and one visible wavelength shared the fourth.

TRACE used its small field of view and rapid cadence to study the evolution and oscillations of coronal loops. These oscillations can only be seen with high-resolution EUV imagers. They are transverse, or kink, oscillations of solar coronal loops that exist only in a magnetically dominated plasma. Observations of kink oscillations of coronal loops provide a seismological probe of the magnitude of the magnetic field and also clues about their rapid damping after excitation. Their typical period of 224 s was well sampled by TRACE and was part of the design parameters for the 12 s cadence of the AIA/SDO full disk images.

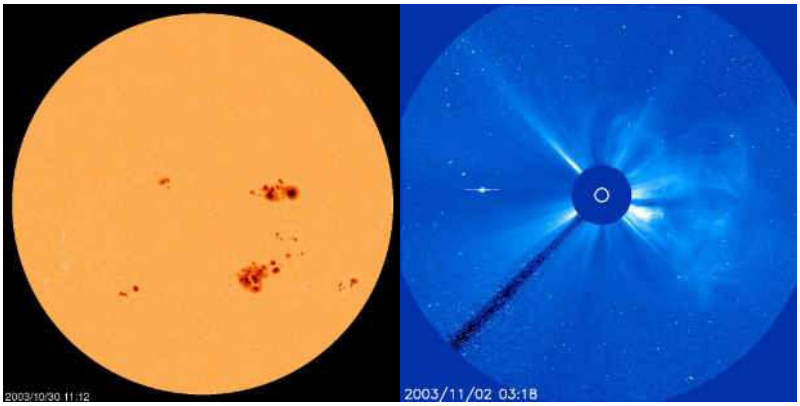

Fig 13. (left) Active regions 486 (in the south) and 488 (in the north) as they looked in a continuum image from MDI/SoHO on 30-Oct-2003. These active regions represent 82% of the sunspot area on this day. Between 19-Oct-2003 and 07-Nov-2003 these active regions produced several X-class flares and large CMEs. (right) The early stages of several of those CMEs seen as the billowing arches on the right side of the Sun. The bright object on the left (with the straight line through it) is the planet Mercury moving behind the Sun. Several proton hits can be seen as short line segments about the image. Courtesy SoHO (ESA & NASA).

4.8 Hinode

Hinode was launched as Solar-B at 2136 UTC on 22-Sep-2006 into a sun-synchronous orbit. Hinode includes an optical telescope (SOT), X-ray telescope (XRT), and an EUV imaging spectrometer (EIS). During almost a decade of observations, Hinode has produced many results about solar flares and the magnetic field that causes them. Two results should be noted, the cause of white light flares and the strength of the polar field. Both of these discoveries were made possible by the SOT's high spatial resolution and high-precision polarimetry.

Watanabe *et al* [39] combined data from Hinode and RHESSI to examine a white-light flare. They showed that solar flare white-light emission comes from the same population of nonthermal electrons as the hard X-rays. The simplest explanation of the observed correlation between white light and hard X-ray emissions is that the two components should originate in the same source region. Analysis of RHESSI and

HMI/SDO data has shown a similar result [40].

Understanding the solar polar magnetic field is extremely important for forecasting solar activity [8]. Before Hinode, it had been thought that the polar magnetic field was made up of weak, diffuse magnetic elements.

The SOT measured the magnetic field strength in the solar polar region and discovered the magnetic field was concentrated in isolated patches with field strengths greater than 1 kG — similar to that of a sunspot [41]. The patches are broadly distributed over the entire polar region. The patches have small areas and have shorter lifetimes when compared to a sunspot.

Those Hinode observations were made during the extremely low solar minimum between Solar Cycles 23 and 24. SOT observations of the polar magnetic field during the maximum of Solar Cycle 24 showed that the northern polar field changed sign two years before the southern polar magnetic field. That these sign changes are not coincident must be related to the evolution of the solar dynamo and is an important clue to how the solar cycle recycles the magnetic field observed during solar maximum.

4.9 STEREO

The two satellites of the Solar Terrestrial Relations Observatory (STEREO A & B) were launched at 0052 UTC on 26-Oct-2006. Their orbits around the Sun cause them to respectively move farther ahead of and fall gradually behind the Earth. This enables stereoscopic imaging of the solar corona and other extended phenomena such as CMEs. Each spacecraft carries EUV and white light imagers whose combined data can follow a CME from the solar surface to the Earth, particle experiments, and radio detectors in four instrument packages.

The orbits of STEREO A & B provide unique views of the Sun. One is stereoscopic images of the Sun, where images from two slightly different viewpoints can be combined into a 3-D view of the Sun. The other is producing images of the Sun from vantage points other than the Earth. This allows scientists to directly monitor the far side of the Sun, instead of deducing the activity on the far side from data gathered near the Earth. The two spacecraft drifted apart and on 6-Feb-2011, they were 180 apart from each other, allowing the entire Sun to be seen at once for the first time. An example of a full-Sun image is shown in Fig 14.

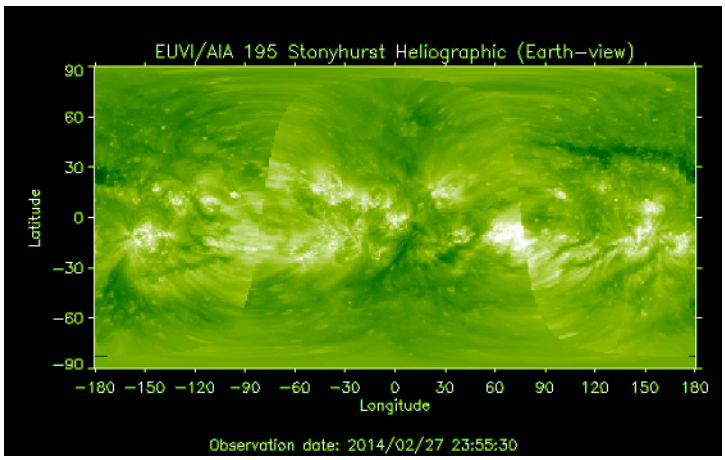

Fig 14. A composite of STEREO A & B 193 Å images with an SDO 193 Å image showing what the entire EUV Sun looked like on 27-Feb-2014. A comparison of the features in the individual images of Fig 7 shows the long dark structure. Courtesy NASA, AIA/SDO, and SECCHI/STEREO.

The imagers on STEREO monitor the far side of the Sun for CMEs. The other instruments measure that plasma when it moves by the spacecraft. On 23-Jul-2012, STEREO-A was in the path of the Solar Storm of 2012 that would have been similar in strength to the Carrington Event of 1859 had it impacted Earth. The unique vantage point of STEREO A allowed it to measure a rare event and proved that we miss at least some of the large events.

One success of the STEREO mission has been to show that multiple vantage points for solar observations are good for research and for space weather forecasters. That success has led to the development of several Sun-Earth L5 missions to continue solar observations from multiple lines of sight.

4.10 SDO

The Solar Dynamics Observatory (SDO) was launched at 1523 UTC on 11-Feb-2010 into an inclined geosynchronous orbit. SDO is unique among science missions in having a continuous data downlink, allowing near-real time data to be made available less than 15 minutes after it is measured [42]. SDO has three instruments, an EUV imager (AIA), magnetogram & Dopplergram instrument (HMI), and an EUV spectral irradiance instrument (EVE). AIA combines a set of iron ions (Fe XVIII at 94 Å, Fe VIII & XXI at 131 Å, Fe IX at 171 Å, Fe XII & XXIV at 193 Å, Fe XIV at 211 Å, and Fe XVI at 335 Å), with the emissions of He II 304 Å to sample many conditions in the corona and chromosphere, including hot flare channels, providing more accurate temperatures [30]. Some of the AIA passbands include spectral lines from several ion states and the combination of channels allows a more accurate determination of temperature than a single ion state.

SDO data has resulted in advances in coronal seismology and large-scale coronal waves propagating across the disk of the Sun. Coronal seismology requires continual data from a large part of the solar disk to ensure the oscillating loops can be identified. They manifest differently in each of the AIA pass bands, which gives clues to their origin and aiding in their interpretation. Large-scale coronal waves appear to emanate from impulsive events such as the filament eruptions that lead to CMEs [43]. Unlike loop oscillations, coronal waves span the solar disk and benefit from multi-point observations to watch as they go over the limb of the SDO field of view and into the view of STEREO.

Solar filaments are large configurations of relatively cool material that are an integral part of the solar coronal field. In quiescent filaments the magnetic field suspends the plasma high above the surface of the Sun. The presence and dynamics of the plasma are often used as precursors of the CMEs that can drive space weather. The continual, high-cadence SDO observations have detailed how filaments are formed by tracing the magnetic field patterns with HMI and the coronal evolution with AIA. The cool material responsible for the filament's appearance has been observed to condense out of the surrounding coronal material [44]. Observations also revealed that matter often drains out of a filament on a time scale of order one day, even as continuing condensation into the filament allows it to survive [45]. The AIA observations also show how the filaments' field configurations destabilize, subject to the buildup of currents within them or the evolution of the surrounding field [e.g., 46]. These results have advanced our scientific understanding of the physical processes governing the Sun and heliosphere.

An accurate optical telescope in space also permits the size and shape of the Sun to be determined. This was done using HMI images by [47], who found the oblateness varied very little over a solar cycle dependence.

They estimated that sizes of a few km (corresponding to 1 mas) is the ultimate resolution of solar viewing. This is much smaller than granules (1.5 Mm) and the pressure scale height in the photosphere (~150 km or 200 mas). Balloon images support the latter figure as the limit future observations should resolve [48].

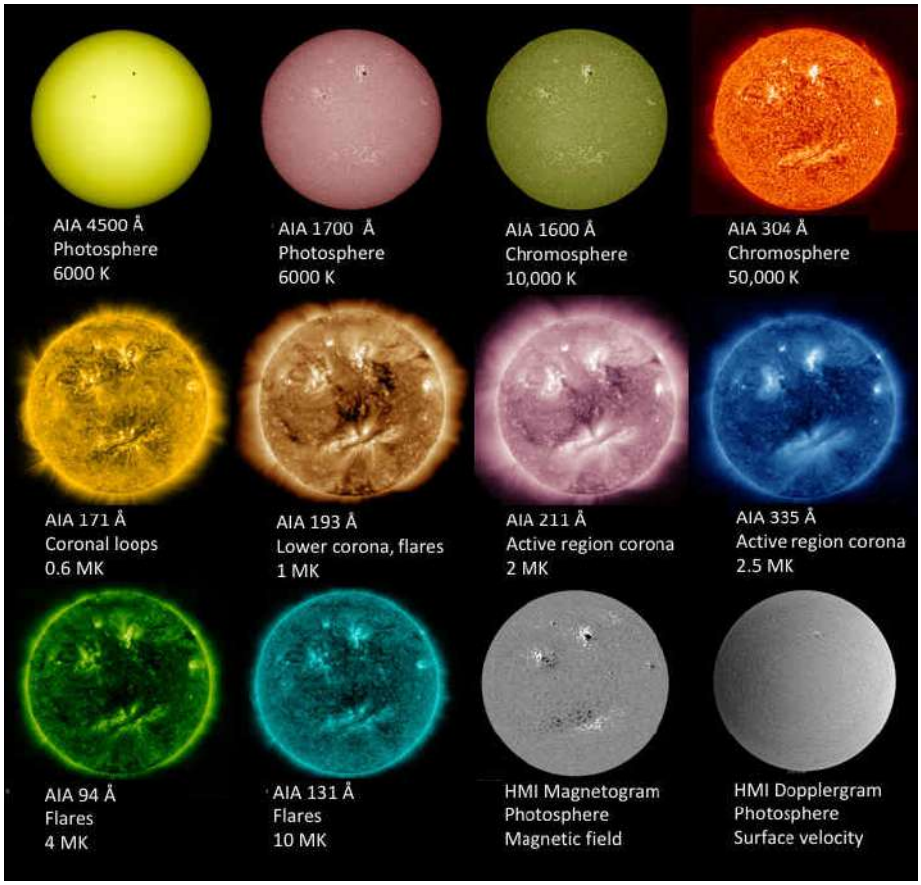

Fig 15. The wavelengths measured by the two imaging instruments on SDO. The passbands of the AIA images, the part of the solar atmosphere it samples, and an estimated temperature of the emitting plasma, are listed under the AIA images. The HMI line-of-sight magnetogram and Dopplergram are also labeled. These images were all taken on 9-Dec-2010 and illustrate the varying appearance of the Sun in the data when there were two active regions in the northern hemisphere and a large filament in the southern. Courtesy of NASA/SDO and the AIA and HMI science teams.

4.11 Atomic Data

Spectral lines of highly-ionized iron, oxygen, and carbon atoms are commonly used to diagnose the properties of the corona. Many of the EUV and X-ray imagers described above use the large number of iron ion states and emission lines for that purpose. Using the ions from a single element for temperature studies removes the effect of possible composition variations between the various parts of the solar atmosphere. The interpretation of those images has driven a need for accurate atomic data of highly-ionized elements. The CHIANTI database was developed to calculate the emission of coronal plasmas [49]. Since the release of CHIANTI v. 1 in 1997, the database has undergone many revisions to include new physics and to allow it to interpret new observations. The common use of iron lines in solar imagers meant that the iron atomic data has received a great deal of attention [50]. Figure 16 shows the dramatic increase in the number of energy levels included for each iron ion state in the CHIANTI v.8 database. The iron ions also span a range of temperatures that includes most of the coronal variations (see the solid line in Fig 16.)

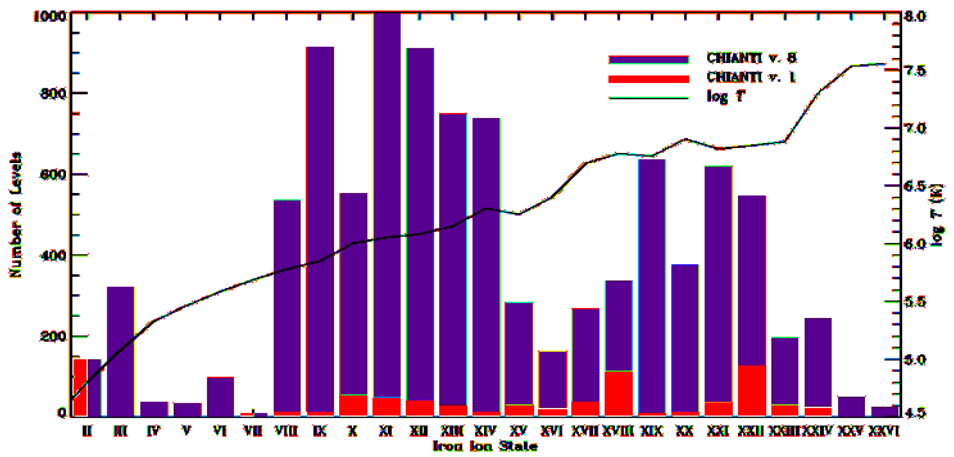

Fig 16. A comparison of the number of energy levels of iron ion states included in the first version of the CHIANTI database (v. 1) with the most recent (v. 8). Two ion states have the same number of levels and are colored as v. 1 and v. 8. The solid line is an estimate of the temperature where each ion level is ionized. Data courtesy of Peter Young.

There are times when the coronal composition markedly departs from the assumed abundances. When a sun-grazing comet is imaged by AIA the emissions have a strong contribution from oxygen lines that then fade as the injected oxygen ionizes and diffuses away from the deposition region [51]. Including these spectral lines in the CHIANTI model improves the agreement of the atomic data with the observations of Comet Lovejoy and may lead to new probes of the coronal density and magnetic field.

5 Future solar observatories

The Sun varies on many timescales and the events that can damage satellites, technology, and humans can happen at any time, so orbits that allow near-continuous observation of the Sun are usually chosen for solar observatories. These include sun-synchronous (Trace and Hinode) and precessing (SORCE, TIMED, and SMM) low-Earth orbits; geosynchronous (SDO and GOES); halo orbits around the Lagrangian L1 point (SoHO, ACE, Wind, and DSCOVR); and deep-space orbits (Helios, STEREO, Ulysses, Solar Probe Plus, and Solar Orbiter). Some of the properties of orbits used for solar observatories are listed in Table 3, including orbits described below.

A solar observatory must be placed into a carefully chosen orbit. Every possible orbit has advantages but most come with difficulties. Three basic constraints determine what orbit to use for a satellite — power, cadence, and telemetry rate. Most solar missions are not limited in the available power because the solar panels can be positioned to be illuminated whenever solar observations are being made. This will become less true as mission orbits move closer to the Sun and the thermal environment becomes more difficult to cope with. To reduce the complexity of these missions it has been proposed that spacecraft flying close to the Sun use RTGs for electrical power. RTGs use thermocouples to convert the heat generated by the decay of Pu-238 into electricity. Because they have no moving parts that can fail or wear out, RTGs are viewed as a highly reliable power option for missions where solar arrays cannot be used. Perhaps a similar thermoelectric generator could convert the Sun's thermal heat into electricity to power a satellite flying close to the Sun while helping to dissipate the incident heat flux.

Table 3. Orbits of solar observatories

Orbit	Distance from Sun (AU)	Orbit period	Data rate
LEO	1	90 min	moderate
LEO Sun-synchronous	1	90 min	moderate
Geosynchronous	1	1 day	high
Earth-Moon L4, L5	1	28 day	high
Earth-Sun L1	0.99	1 year	moderate
Earth-Sun L5 (trailing)	1	1 year	moderate
Heliocentric, high inclination	var.	var.	low
Heliocentric, ecliptic plane	var.	var.	moderate
Heliosynchronous	0.169	25.4 d	low
Sun-sampling	var.	var.	moderate

An orbit must optimize the fraction of the orbit during which the Sun can be observed and how often a downlink station is visible to receive the data. All orbits except geosynynchronous are subject to the rotation of the Earth continually moving downlink stations into and out of view. The proximity of the Earth's surface makes low-Earth orbits particularly sensitive to the location of ground stations. The data downlink rate in low-Earth orbits is increased by higher inclination, up to the 98° inclination of the Sun-synchronous orbit. In this case, high inclination means access to the polar ring of downlink stations. Deep space orbits require the satellite to carry powerful transmitters to overcome the loss caused by the distance to the Earth. Laser-based communications are being tested to provide higher data transfer speeds for upcoming missions.

Orbits that are not currently in use but could be used for future solar observatories include the Earth-Moon L5 Lagrange point, some of the Sun-Earth Lagrange points, heliosynchronous, and solar-sampling orbits (see Fig 17). The first orbit becomes very useful for solar observations if a relay station is placed on the Moon. The satellite would be in constant contact with the station that would use a powerful transmitter and large antenna to forward the data to Earth.

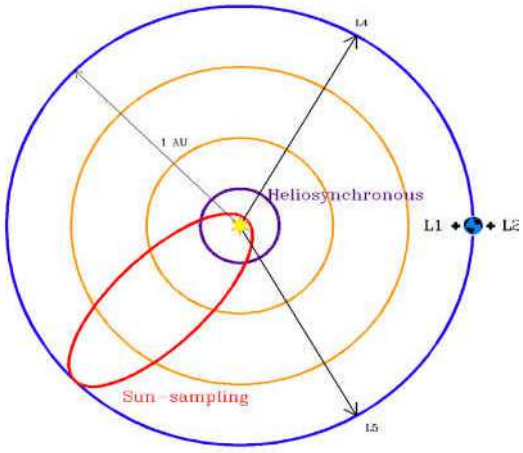

Fig 17. A schematic of orbits that could be used for future solar observatories. The view is from above the ecliptic. The Sun-Earth Lagrange points are noted. A sun-grazing orbit is shown as the red tilted ellipse and the heliosynchronous orbit as a purple circle. The orbits of Mercury and Venus are shown as circles drawn with a radius of the respective semi-major axis. The Earth's orbit is drawn as a blue circle at 1 AU. Although the orbits are roughly to scale, the sizes of the Sun and Earth and the positions of L1 and L2 are not.

The Sun-Earth Lagrange points are locations for current and future solar observatories. The Sun-Earth L1 Lagrange point already hosts SoHO, ACE, Wind, and DSCOVR. This is an unstable point in space, so a halo orbit perpendicular to the ecliptic is used for station keeping. Solar observatories at the L1 point have been highly productive with long lifetimes.

A satellite at the Sun-Earth L2 point could use the Earth to block most of the Sun, reducing the heat load and perhaps allowing a coronagraph to have a smaller occulting disk. From this vantage point the Earth spans 29.2′ while the Sun spans 31.5′. The larger occulting disk in orbiting coronagraphs allows for misalignments during launch that could increase the scattered light inside the instrument. Using the Earth as a first occulting disk may reduce the incident light that is then scattered.

The Sun-Earth L5 point is being considered for several future solar observatories. A spacecraft at this point would see solar longitudes that are about to rotate into the view of the Earth, increasing the visible area of the Sun by ~60°. Coronagraphs on the Sun-Earth line see incoming CMEs as rings around the occulter disk or halo CMEs. This limits the predictive capability of the models for possible impact on the Earth. The side view of halo CMEs from this location will improve both our understanding of CMEs and our ability to predict whether they will strike the Earth. It is 1 AU from the Earth, which limits the data rate if adequate receivers are not placed around the Earth. It is also subject to perturbations that will cause the satellite to wander in space. This would require either accepting these perturbations in the operations plan or using an active control of the position.

Another future orbit is the heliosynchronous orbit. As defined here, it is a circular orbit with a period matching the sidereal rotation rate of the active latitudes (25.4 d). This orbit has a semi-major axis of 0.169 AU or 36 R_{SUN}. It has a field of view of 88°, similar to satellites far from the Sun. The orbit lies within the orbit of Mercury and the heat load is 35 times that at 1 AU. This means the sunlit side of a non-rotating satellite could reach temperatures of ~1000 K, above the melting point of aluminum.

The telemetry link for this orbit is complicated by the transits of the satellite across the face of the Sun. During those times the transmitter signal will be overwhelmed by the solar flux. The maximum elongation of the satellite is about 10°, meaning it will be visible from the ground for about an hour before sunrise or after sunset (much like Mercury), which means the Earth could block the solar interference. The major advantage of this orbit is the sampling of a single longitude range for helioseismic studies, eliminating the need to track patches from limb to limb and increasing the sampling time of that longitude range. This would permit the helioseismic sampling of deeper depths in the Sun, possibly uncovering the ultimate seat of the solar dynamo. It also sits close enough to the Sun to sample the Parker spiral of many velocities before they disperse further out, allowing the fast and slower solar wind particles from the same region to be measured soon after they leave the Sun. Attaining this orbit would require a total $\Delta v \sim 50$ km/s to first drop the perihelion from 1 AU to 0.169 AU and then to circularize the orbit at that distance from the Sun.

The solar-sampling orbit is the last to be considered. We have seen small sungrazing comets pass close to the solar surface and, in one case, survive perihelion passage. Is it possible to send a probe into the photosphere of the Sun to measure the compositions and magnetic field of the corona, chromosphere, and photosphere on the inbound and outbound legs? The heat load would be tremendous as the spacecraft skims along the solar surface. What mechanism could dissipate that heat load and keep the satellite and instruments at a comfortable temperature? Sungrazing comets are able to approach close to the Sun by evaporative cooling. Sublimating water ice absorbs the incoming heat radiation and keeps the comet surface at a comfortable temperature. Thermal stresses and tidal forces fracture some of the comets as they approach perihelion. While those effects can be handled by an appropriate structure, dissipating the heat load and not distorting the plasma measurements would be a real challenge for these orbits. The goal is an *in situ* composition measurement that could help us understand the radiative transfer algorithms that seem to require changes in the composition from time to time.

The data from these orbits would have to be retrieved far from perihelion. Attaining this orbit would require a $\Delta v \sim 30$ km/s to drop the perihelion from 1 AU to 4.7×10^{-3} AU. The period of this model orbit is 0.356 yr, so a recovery is possible after a year and three samples of the Sun. These simple orbital calculations neglect the drag force as the satellite passes close to the Sun.

6 Planned Missions

There are a number of missions being built to study the Sun over the next decade. Others are in the planning stages.

6.1 GOES-R Series

The first satellite in the GOES-R series is scheduled to launch in October 2016 for the National Oceanic and Atmospheric Administration (NOAA). It will carry two solar instruments, the Solar Ultraviolet Imager (SUVI) and EUV and X-Ray Irradiance Sensors (EXIS). The Space Environment In-Situ Suite (SEIS) will measure the particles and fields at the geosynchronous orbit, which are a mixture of solar and terrestrial influences.

SUVI will provide 1-minute cadence images in six EUV bandpasses using normal incidence, multilayer mirrors similar to those in the AIA telescopes. The imaged wavelengths are Fe XVIII at 94 Å, Fe VIII & XXI at 131 Å, Fe IX at 171 Å, Fe XII & XXIV at 195 Å, Fe XV at 284 Å, and He II 304 Å.

EXIS comprises two instruments, the Extreme Ultraviolet Sensor (EUVS) and the X-Ray Sensor (XRS). EUVS will provide the EUV spectral irradiance needed to monitor the solar output and drive thermospheric models. The XRS will monitor the solar X-ray output and classify solar flares.

6.2 Solar Probe Plus

The Solar Probe Plus (SPP) mission is being built by NASA to use seven Venus flybys to reduce the perihelion distance to a new record of 9.5 R_{SUN} (0.044 AU). SPP will carry four particle & field instruments, a radio instrument, a coronagraph, and a heliospheric imager. This instrument suite will provide information about the solar wind close to the Sun, allowing the internal effects as the material moves through the solar system to be distinguished from the initial conditions. During some orbits the satellite will move with the solar wind that is being sampled.

SPP will sample particles closer to the solar acceleration region than any other mission. In this region it may be possible to measure the effects of the dust on the acceleration of the solar wind.

6.3 Solar Orbiter

Solar Orbiter (SO) is being built by the European Space Agency and NASA. It will use a series of gravity-assist maneuvers at Earth and Venus to reach a moderate-inclination orbit with a maximum heliographic inclination of 25°. Subsequent maneuvers in an orbit resonant with Venus will result in an operational orbit with a perihelion radius of 0.28 AU and a period of 168 days. During the extended mission, additional Venus fly-bys could allow the orbital inclination to increase to about 34°. The main scientific activity will take place during the near-Sun encounters and high-latitude parts of each orbit.

SO will carry three particle & field instruments, a radio instrument, two EUV imagers, an X-ray imager, a coronagraph, and a heliospheric imager. This instrument suite will provide information about the solar wind close to the Sun, allowing the internal effects as the material moves through the solar system to be distinguished from the initial conditions.

6.4 Aditya-1

The Aditya-1 spacecraft being built by the Indian Space Research Organisation (ISRO) will carry six instruments into an orbit at the Sun-Earth L1 Lagrange point. The main instrument is a visible emission line coronagraph, with a UV imager, two X-ray spectrometers, and two plasma instruments added for the current mission.

6.5 INTERHELIO-Zond

The Federal Space Program of the Russian Federation is developing the INTERHELIO-Zond project to fly near the Sun. It is scheduled to launch in 2022 into a high-inclination orbit with a perihelion distance of 21×10^6 km (0.14 AU). INTERHELIO-Zond will travel close to the Sun to solve problems of solar corona heating, the acceleration of the solar wind, and the origin of the solar flares and coronal mass ejections. One unique aspect is the measurement of energetic neutrons (0.01–5 MeV, 20–100 MeV) to evaluate the origin and spectral distribution of those neutrons.

6.6 DSO, SPORT, and ASO-S

The Chinese National Space Administration (CNSA) has been developing several solar satellites that could be flown in the next few years. One, the Deep-space Solar Observatory (DSO), contains a 1-m telescope to be placed at the Sun-Earth L1 point, would be the largest aperture solar telescope in orbit. The Advance Solar Observatory in Space (ASO-S) is another CNSA satellite under development for a sun-synchronous orbit. Instruments include a full disc vector magnetograph, a Lα imager, and a hard X-ray imager. Scheduled to be launched in 2022.

The CNSA Solar Polar ORbit Telescope (SPORT) is intended to be launched into a high-inclination solar orbit ($i > 60°$) using a gravity assist from Jupiter. The planned perihelion is ~ 0.7 AU with an aphelion between 2 and 5 AU. The instrumentation on SPORT includes a heliospheric imager, coronagraph, magnetograph, a Lα imager, a variety of particle detectors, and radio wave experiments. Launch of SPORT could be before 2025.

7 The Future

Space-based observations of the Sun will be essential in providing knowledge of solar activity and the Space Weather it creates. Distinguishing between the various theories of coronal heating or filament eruption will require the data produced by solar observatories in space. Scientific studies of that data provide insight into how solar activity is formed, with a goal of predicting that activity in the short and long-term. What are we missing in the present fleet and what new measurements should we make?

1. Views of the Sun away from the ecliptic would allow the polar regions to be more properly sampled. These regions are a consistent source of the high-speed solar wind. The polar magnetic field is an important part of the solar dynamo and measurements from a high-inclination orbit would better resolve the magnitude and direction of that field. Solar Orbiter will carry instruments to measure the solar wind particles and magnetic field at higher inclinations as well as imagers to measure the coronal back-scattered emissions. But a polar orbit of the Sun with imagers that produce the magnetograms and Dopplergrams needed to track the polar component of the solar dynamo are not yet in the mix.
2. Are there limits to the spatial, spectral or temporal resolutions needed to understand the evolution of the solar magnetic field? There are indications that a resolution of a few mas (about 100× the current space-based resolution) is the ultimate spatial resolution needed in solar observations. A diffraction limited telescope operating at 304 Å would need a diameter of 6.5 m to satisfy the Rayleigh criterion for this resolution. Such high spatial resolution comes at a loss of available photons from the surface. The Daniel K. Inouye Solar Telescope (DKIST)[7] being constructed on Haleakala, Hawai‘i uses a 4.2 m primary telescope and adaptive optics to reach has a spatial resolution of ~ 22 mas. But each image covers less than 0.5% of the solar surface. DKIST will serve as a microscope of the solar surface while full-disk imagers provide the context of the surrounding plasma.

   It is a little easier to establish the ultimate temporal resolution as that necessary to resolve flares, the most rapid phenomena we see on the Sun. The spectral resolution is similar in that it must resolve the

[7] http://dkist.nso.edu

many spectral lines created by the hot flare plasma. Observations of some emission lines must resolve a narrow reversal in the core of the line. If such rapid cadences and spectral resolution are maintained across the full disk of the Sun all other phenomena will be resolved. Building satellites with nested resolutions each sufficient to address one set of events might be a more cost effective solution.

An example of a needed set of observations is high-resolution spectroscopy of the X-ray wavelengths, especially during flares. Much progress was made in flares when P78-1 showed the Doppler shifts of the chromospheric emission caused by flares. Improving on these observations will reveal how energy flows within the flaring region.

3. How close to the Sun can we go to obtain in situ samples of plasma and electromagnetic fields? How close do we need to go to understand the solar dynamo and magnetic field? The Helios spacecraft measured the solar wind at a record heliocentric distance of 0.29 AU on 17-Apr-1976. A few spacecraft are planned to approach closer to the Sun, but no planned mission will reach the solar wind acceleration region that lies a few solar radii above the surface of the Sun.
4. The elemental abundances are one outstanding issue in our understanding of the Sun. Spectroscopic measurements have been revised several times. For example, recent reports showed that the abundances of C, N, O, and Ne should be reduced from previous lists, while the abundance of Fe remained about the same [52, 53]. When used in stellar evolution models these abundances do not reproduce the helioseismic frequencies used to understand the solar interior [54]. The First-Ionization Potential (FIP) effect confuses the abundance measurements in the corona and solar wind because the coronal abundances of neutral elements with small ionization potentials ($\chi < 10$ eV) are enhanced compared to the photospheric abundances [55]. Photospheric abundances are determined by spectral line analysis and direct sampling of the photosphere might reduce the ambiguity of those measurements. Can in situ samples of the corona, chromosphere, and photosphere be obtained to help our understanding of the composition of the Sun?

These scientific topics require new instrumentation and satellites. Some topics would benefit from quickly placing current instrumentation into new classes of orbits, or extend the measurements to different altitudes in the solar atmosphere. As an example, helioseismology and magnetography would benefit from several innovations.

1. Helioseismology would benefit from satellites in orbits at higher inclinations and in the heliosynchronous orbits. Global oscillation mode amplitudes measured from near the ecliptic have systematic variations that can be understood only by making similar measurements from higher inclination orbits. Deep time-distance helioseismology tracks patches of the Sun as they rotate past the observer to look deep inside the Sun. Producing Dopplergrams from a heliosynchronous orbit would remove the rotational effects and allow a deeper look inside the Sun. Analyzing polar Dopplergrams would remove the projection effects that are always present when observing the Sun from the ecliptic and lead to a better understanding of the flows inside the Sun that are a major part of the solar dynamo.
2. Helioseismology of the chromosphere and corona as well as different heights in the photosphere. As the altitude increases the plasma oscillations become more dominated by magnetic field effects. Such measurements would continue the studies started with SMM and that continued with the AIA/SDO 1600 Å passband [56]. The differing wavelengths mean acoustic power is visible at all locations on the disk. Where the photosphere is dark (such as a sunspot umbra) the UV channels may be bright and vice versa.
3. Polarization-sensitive spectroscopy of the Mg II h&k 2800 Å, H I Ly-α 1216 Å, and He II 304 Å could provide measurements of the chromospheric magnetic field [57, 58]. Unlike the circularly polarized Zeeman splitting used in the photospheric lines, these UV lines are sensitive to the Hanle effect, which allows a weaker field strength to be measured. By working with the cores of these lines the chromospheric

and transition region effects are emphasized.

4. The Sun-Earth L5 Lagrange point offers an orbit for a deep-space solar observatory that increases the observable surface of the Sun by 33% and provides space weather forecasters advance knowledge about active regions before they come into view of the Earth. The payload would be EUV imagers, coronagraph, and magnetograms.

   One useful technology would be the continued development of CMOS detectors as active pixel sensors that can readout selected pixels. During flares the pixels imaging the flare can be read out faster than the pixels imaging the dimmer regions of the Sun. This would overcome the effects of simply reducing the exposure time, where the flaring region is still saturated and the rest of the Sun is underexposed.

8 Concluding Remarks

Space-based data has been at the forefront of major advances in our understanding of the solar dynamo and solar activity. The near-continuous cadence of high-quality Dopplergrams and magnetograms has allowed researchers to probe ever deeper into solar interior. As a result, we can determine several patterns of plasma motion inside the solar convection. The patterns change as the sampling interval is varied; from multiple cells in latitude for short intervals to multiple cells in radius for long intervals.

The solar corona spectacularly revealed by rare total solar eclipses is seen everyday in vivid detail by EUV and X-ray sensors in space. The phenomena of coronal heating is imaged by space-based detectors, including the spectroscopic signatures in UV spectral lines. Without the GOES X-ray sensors we would have no way to classify flares over four sunspot cycles and counting.

Looking out from the Solar System, those same data will provide clues to many astrophysical problems. Researchers in accretion, stellar flares, and convection theory, and stellar dynamos all use the data from solar satellites to advance their work.

Ground-based observatories will never provide a substitute for the space-based information that has become an indispensable tool for solar scientists and space weather forecasters. Solar observatories in space will continue to provide useful solar data as long as they keep flying.

Acknowledgments

This work was supported by NASA and the Solar Dynamics Observatory. The TSI composite is courtesy of PMOD/WRC, Davos, Switzerland, and is updated with continuing data from the VIRGO Experiment on SoHO. It is available from ftp://ftp.pmodwrc.ch/pub/data/irradiance/ composite/composite_42_64_1510.dat. The International Sunspot Number values are from the WDC-SILSO, Royal Observatory of Belgium, Brussels. F10.7 values are courtesy of the Dominion Radio Astronomy Observatory, Penticton, British Columbia, Canada and downloaded from the National Geophysical Data Center (NGDC) in Boulder, Colorado.

Reference

1. Tousey R, Strain C V, Johnson F S, Oberly J J, *Astron J*, 52(1947)158-159.
2. Rense W A, *Phys Rev*, 91(1953)299-302.
3. Mercure R, Miller S C, Rense W A, Stuart F, *J Geophys Res*, 61(1956)5573.
4. Banks P M, Kockarts G, *Aeronomy*, (NY: Academic Press), 1973.
5. Tousey R, *Astrophys J*, 149(1967)239-252.
6. Dennis B, Milligan R, 2010 *Scholarpedia*, 5(7), 6139 revision #143457, http://www.scholarpedia.org/article/Solar_Satellites
7. Hinteregger H E, Fukui K, Gilson B R, *Geophy Res Lett*, 8(1981)1147-1150
8. Schatten K, *Geophys Res Lett*, 32(2005)L21106

9. McComas D, Allegrini F, Bagenal F, Casey P, Delamere P, Demkee D, Dunn G, Elliott H, Hanley J, Johnson K, Langle J, Miller G, Pope S, Reno M, Rodriguez B, Schwadron N, Valek P, Weidner S, *Space Sci Rev*, 140(2008)26-313.
10. Bougeret J L, Goetz K, Kaiser M L, Bale S D, Kellogg P J, Maksimovic M, Monge N, Monson S J, Astier P L, Davy S, Dekkali M, Hinze J J, Manning R E, Aguilar-Rodriguez E, Bonnin X, Briand C, Cairns I H, Cattell C A, Cecconi B, Eastwood J, Ergun R E, Fainberg J, Hoang S, Huttunen K E J, Krucker S, Lecacheux A, MacDowall R J, Macher W, Mangeney A, Meetre C A, Moussas X, Nguyen Q N, Oswald T H, Pulupa M, Reiner M J, Robinson P A, Rucker H, Salem C, Santolik O, Silvis J M, Ullrich R, Zarka P, Zouganelis I, *Space Sci Rev*, 136(2008)487-528.
11. De Pontie B, McIntosh S W, Carlsson M, Hansteen V H, Tarbell T D, Boerner P, Martinez-Sykora J, Schrijver C J, Title A M, *Science*, 331(2011)55-58.
12. De Pontieu B, Title A M, Lemen J R, Kushner G D, Akin, D J, Allard B, Berger T, Boerner P, Cheung M, Chou, C, Drake J F, Duncan D W, Freeland S, Heyman G F, Hoffman C, Hurlburt N E, Lindgren R W, Mathur D, Rehse R, Sabolish D, Seguin R, Schrijver C J, Tarbell T D, W¨ ulser J -P, Wolfson C J, Yanari C, Mudge J, Nguyen-Phuc N, Timmons R, van Bezooijen R, Weingrod I, Brookner R, Butcher G, Dougherty B, Eder J, Knagenhjelm V, Larsen S, Mansir D, Phan L, Boyle P, Cheimets P N, DeLuca E E, Golub L, Gates R, Hertz E, McKillop S, Park S, Perry T, Podgorski W A, Reeves K, Saar S, Testa P, Tian H, Weber M, Dunn C, Eccles, S, Jaeggli S A, Kankelborg C C, Mashburn K Pust N, Springer L, Carvalho R, Klein L, Marmie J, Mazmanian E, Pereira T M D, Sawyer S, Strong J, Worden S P, Carlsson M, Hansteen V H, Leenaarts, J, Wiesmann M, Aloise J, Chu K -C, Bush R I, Scherrer P H, Brekke P, Martinez-Sykora J, Lites B W, McIntosh, S W, Uitenbroek H, Okamoto T J, Gummin M A, Auker G, Jerram P, Pool P, Waltham N, *Solar Phys*, 289(2014)273-2779; http://adsabs.harvard.edu/abs/2014SoPh..289.2733D
13. Rottman G, *Solar Phys*, 230(2005)7-25.
14. Kosugi T, Makishima K, Murakami T, Sakao T, Dotani T, Inda M, Kai K, Masuda S, Nakajima H, Ogawara Y, Sawa M, Shibasaki K, *Solar Phys*, 136(1991)17-36.
15. Garrett D L, Tousey R, *Appl Opt*, 16(1977) 98-903.
16. Vaiana, G S, van Speybroeck L, Zombeck M V, Krieger A S, Silk J K, Timothy A, *Space Sci Instrument*, 3(1977) 19-76.
17. Reeves E M, Huber M C E, Timothy J G, *Appl Opt*, 16(1977)837-848.
18. Underwood J H, Milligan J E, deLoach A C, Hoover R B, *Appl Opt*, 16(1977)858-869.
19. Tousey R, Bartoe J -D F, Brueckner G E, Purcell J D, *Appl Opt*, 16(1977)870-878.
20. Bartoe J -D F, Brueckner G E, Purcell J D, Tousey R, *Appl Opt*, 16(1977)87-886.
21. Crockett W R, Patterson N P, Purcell J D, Schumacher R J, Tousey R, *Appl Opt,* 16(1977)893-897.
22. Tsuneta S, Acton L, Bruner M, Lemen J, Brown W, Caravalho R, Catura R, Freeland, S, Jurcevich B, Morrison M, Ogawara Y, Hirayama T, Owens J, *Solar Phys*, 136(1991)37-67.
23. Hill S M, Pizzo V J, Balch C C, Biesecker D A, Bornmann P, Hildner E, Lewis L D, Grubb R N, Husler M P, Prendergast K, Vickroy J Greer S, Defoor T, Wilkinson D C, Hooker R, Mulligan P, Chipman E, Bysal H, Douglas J P, Reynolds R, Davis J M, Wallace K S, Russell K, Freestone K, Bagdigian D, Page T, Kerns S, Hoffman R, Cauffman S A, Davis M A, Studer R, Berthiaume F E, Saha T T, Berthiume G D, Farthing H, Zimmermann F, *Solar Phys*, 226(2005)255-281.
24. Pizzo V J, Hill S M, Balch C C, Biesecker D A, Bornmann P, Hildner E, Grubb R N, Chipman E G, Davis J M, Wallace K S, Russell K, Cauffman S A, Saha T T, Berthiume G D, *Solar Phys*, 226(2005)283-315.
25. Delaboudiniere J -P, Artzner G E, Brunaud J, Gabriel A H, Hochedez J F, Millier F, Song, X Y, Au B, Dere K P, Howard R A, Kreplin R, Michels D J, Moses J D, Defise, J M, Jamar C, Rochus P, Chauvineau, J P, Marioge, J P, Catura R C, Lemen J R, Shing L, Stern R A, Gurman, J B, Neupert W M, Maucherat A, Clette F, Cugnon P, van Dessel E L, *Solar Phys*, 162(1995)291-312.
26. Howard R A, Moses, J D, Vourlidas A, Newmark J S, Socker D G, Plunkett S P, Korendyke C M, Cook J W, Hurley A, Davila J M, Thompson W T, St Cyr O C, Mentzell E, Mehalick K, Lemen J R, Wuelser J P, Duncan D W, Tarbell T D, Wolfson C J, Moore A, Harrison R A, Waltham N R, Lang J, Davis C J, Eyles C J, Mapson-

Menard H, Simnett G M, Halain J P, Defise J M, Mazy E, Rochus P, Mercier R, Ravet M F, Delmotte F, Auchere F, Delaboudiniere J P, Bothmer V, Deutsch W, Wang D, Rich N, Cooper S, Stephens V, Maahs G, Baugh R, McMullin D, Carter T, *Space Sci Rev*, 136(2008)67115.

27. Wuelser J -P, Lemen J R, Tarbell T D, Wolfson, C J, Cannon, J C, Carpenter B A, Duncan D W, Gradwohl G S, Meyer S B, Moore A S, Navarro R L, Pearson J D, Rossi G R, Springer L A, Howard R A, Moses J D, Newmark J S, Delaboudiniere J -P, Artzner G E, Auchere F, Bougnet M, Bouyries P, Bridou F, Clotaire J -Y, Colas G, Delmotte F, Jerome A, Lamare M, Mercier R, Mullot M, Ravet M -F, Song X, Bothmer V, Deutsch W, in "telescopes and Instrumentation for Solar Astrophysics", eds S Fineschi, M A Gummin, *SPIE Conf Ser*, 5171(2004)111-122; http://adsabs.harvard.edu/abs/2004SPIE.5171..111W
28. Seaton D B, Berghmans D, Nicula B, Halain J -P, De Groof A, Thibert T, Bloomfield D S, Raftery C L, Gallagher P T, Auch`ere F, Defise J -M, D'Huys E, Lecat J -H, Mazy E, Rochus P, Rossi L, Schühle U, Slemzin V, Yalim M S, Zender J, *Solar Phys*, 286(2013)43-65
29. Halain J -P, Berghmans D, Seaton D B, Nicula B, De Groof A, Mierla M, Mazzoli A, Defise J -M, Rochus P, *Solar Phys*, 286(2013)67-91.
30. Lemen J R, Title A M, Akin D J, Boerner P F, Chou C, Drake J F, Duncan D W, Edwards C G, Friedlaender F M, Heyman G F, Hurlburt N E, Katz N L, Kushner G D, Levay M, Lindgren R W, Mathur D P, McFeaters E L, Mitchell S, Rehse R A, Schrijver C J, Springer L A, Stern R A, Tarbell T D, Wuelser J -P, Wolfson C J, Yanari C, Bookbinder J A, Cheimets P N, Caldwell D, Deluca E E, Gates R, Golub L, Park S, Podgorski W A, Bush R I, Scherrer P H, Gummin M A, Smith P, Auker G, Jerram P, Pool P, Soufli R, Windt D L, Beardsley S, Clapp M, Lang J, Waltham N, *Solar Phys*, 275(2012)17-40; http://adsabs.harvard.edu/abs/2012SoPh..275...17L
31. St Cyr O C, Fleck B, Davila J M, *EOS Trans AGU*, 95(2014)369-370.
32. Pesnell W D, *Space Weather*, 14(2016)1-14.
33. Willson R C, Hudson H S, *Nature*, 351(1991)42-44.
34. Hickey J R, Alton B M, Kyle H L, Hoyt D V, *Space Sci Rev*, 48(1989)321-342.
35. Frohlich C, *Space Science Rev*, 125(2006)53-65.
36. Khomenko E, Collados M, *Liv Rev Sol Phys*, 12(2015)6.
37. von Steiger R, Zurbuchen T H, McComas D J, *Geophys Res Lett*, 37(2010)L22101.
38. Gizon L, Birch A C, *Living Rev Solar Phys*, 2(2005)6.
39. Watanabe K, Krucker S, Hudson H, Shimizu T, Masuda S, Ichimoto K, *Astrophys J*, 715(2010)651-655.
40. Kuhar M, Krucker S, Martınez Oliveros J C, Battaglia,M, Kleint L, Casadei D, Hudson H S, *Astrophys J*, 816 (2016)6.
41. Shimojo M, Tsuneta S, *Astrophys J Lett*, 706(2009)L145-L149.
42. Pesnell W D, Thompson B J, Chamberlin P C, *Solar Phys*, 275(2012)315.
43. Liu W, Ofman L, *Solar Phys*, 289(2014)3233-3277.
44. Berger T E, Liu W, Low B C, *Astrophys J Lett*, 758(2012)L37.
45. Liu W, Berger T E, Low B C, *Astrophys J Lett*, 745(2012)L21.
46. Su Y, van Ballegooijen A, *Astrophys J*, 764(2013)91.
47. Kuhn J R, Bush R, Emilio M, Scholl I F, *Science*, 337(2012)1638-1640.
48. Solanki S K, Barthol P, Danilovic S, Feller A, Gandorfer A, Hirzberger J, Jafarzadeh S, Lagg A, Riethmuller T L, Schussler M, Wiegelmann T, Bonet J A, González M J M, Pillet V M, Khomenko E, Yelles Chaouche L, Iniesta J C D T, Domingo V, Palacios J, Knolker M, González N B, Borrero J M, Berkefeld T, Franz M, Roth M, Schmidt W, Steiner O, Title A M , in 4th Hinode Science Meeting: Unsolved Problems and Recent Insights, (eds) L Bellot Rubio, F Reale, M Carlsson, M , *Astron Soc Pacific Conf Ser*, 455(2012)143-153.
49. Dere K P, Landi E, Mason H E, Monsignori Fossi B C, Young P R, *Astron Astrophys Suppl Ser*, 125(1997)149-173.

50. Del Zanna G, Dere K P, Young P R, Landi E, Mason H E, *Astron Astrophys*, 582(2015)A56.
51. Pesnell W D, Bryans P, *Astrophys J*, 785(2014)50.
52. Asplund M, Grevesse N, Sauval A J, Scott P, *Ann Rev Astron Astrophys*, 47(2009)481-522.
53. Grevesse N, Asplund M, Sauval A J, Scott P, in Progress in Physics of the Sun and Stars: A New Era in Helio- and Asteroseismology, (eds) H Shibahashi, A E Lynas-Gray, *Astron Soc Pacific Conf Ser*, 479(2013)481-484.
54. Gough D, *Solar Phys*, 287(2013)9-41.
55. Laming J M, *Living Rev Solar Phys*, 12(2015)2.
56. Howe R, Jain K, Bogart R S, Haber D A, Baldner C S, *Solar Phys*, 281(2012)533-549.
57. Belluzzi L, Trujillo Bueno J, Stepan J, *Astrophys J Lett*, 755(2012)L2.
58. Belluzzi L, Trujillo Bueno J, *Astrophys J Lett*, 750(2012)L11.

[*Received*: 15.2.2016; *accepted*: 13.3.2016]